Relating Extreme Temperature and Precipitation to Improve IDF Curve Estimates for Ontario in Response to Climate Change

by

Hiralben Desai

A thesis

presented to the University of Waterloo

in fulfillment of the

thesis requirement for the degree of

Masters of Applied Science

in

Civil Engineering (Water)

Waterloo, Ontario, Canada, 2017

Author's Declaration

I hereby declare that I am the sole author of this thesis. This is a true copy of the thesis, including any required final revisions, as accepted by my examiners.

I understand that my thesis may be made electronically available to the public.

_____

Abstract

Events of extreme precipitation have a huge influence on society. They cause flooding, erosion, and threaten infrastructure, transportation, and safety. Precipitation extremes have increased over the last century (Alexander *et al.*, 2006; Westra *et al.*, 2014), and these changes are the outcome of anthropogenic climate change (Min *et al.*, 2011).

Precipitation extremes are expected continue their increase as the climate warms (Trenberth *et al.*, 2003; Groisman *et al.*, 2005, Emori and Brown, 2005). Precipitation extremes are expected to increase primarily because a warmer atmosphere can absorb more moisture. The increase in the moisture capacity of the atmosphere occurs at a rate given by the Clausius-Clapeyron relation (CCR)—approximately 7% per degree Celsius of temperature increase. The present study combines atmospheric thermodynamics, temporal trends, and interpolated physiographic parameters to forecast extreme precipitation. This provides a new paradigm that characterizes rainfall series, is sensitive to environmental attributes, and thus reflects climate change.

This model is called the Waterloo Interpolator – Topography, Temperature, Time (WIT3). The model preserves a linear time trend from the Regional Trend Analysis (RTA) that Soulis *et al.* (2016) previously developed. WIT3 is compared with observations from the Meteorological Service of Canada (MSC). It is also compared to existing models, such as RTA and Ontario Climate Change Data Portal (OCCDP) models, for the historical period of 1960-2010. In these comparisons, WIT3 best matches the empirical distribution of Ontario weather stations. The extreme precipitation is forecasted up to 2099 using the WIT3 model, and is downscaled and bias corrected with temperature data from Global Climate Models (GCMs).

I have also considered different Representative Concentration Pathways (RCP), or greenhouse gas (GHG) scenarios, to assess the inherent uncertainty of prediction using various GCM-RCP ensembles.

Results revealed that, in the future, the frequency of the current design storms will almost double for all recurrence intervals and durations. Precipitation trends show an increase, especially after 2070. The increase in precipitation intensity is greater for smaller events, especially for the 5 y and 10 y storms, relative to the more severe storm events, such as the 50 y and 100 y storms.

Acknowledgements

I express my sincere gratitude to my supervisor, Dr. E.D. Soulis, whose expertise, understanding, and patience added considerably to my graduate experience. I cannot forget that, he is the only person who trusted me in this new country, and gave me this golden opportunity to contribute my share for the betterment of my fellow residents of Ontario. I would always look to him for inspiration and to motivate myself to keep going in the worst conditions.

I also extend my thanks to my reviewers, Dr. J. Craig and Dr. M. Pandey, whose time and effort helped improve my thesis. I thank all the faculty members and staff in the University of Waterloo's Department of Civil and Environmental Engineering who offered their best to help me in my journey towards professional excellence.

I also acknowledge with sincere gratitude Graham, Neal, Ali, Camron, Jilong, and Setareh who helped me sail smoothly through each phase of my research with their support. It would not be possible for me to carry out this research without support of my family and friends. My husband, Kashyap, and daughter, Hetvi, showed great support as I completed my graduate studies. I am also indebted to my parents, who believed in me, and kept motivating me throughout.

Finally, I cannot imagine myself addressing one of the most important global issues, flooding, without the direction, motivation, and strength provided by the Almighty.

Table of Contents

Contents

List of Figures

List of Tables

List of Abbreviations

AR4:A1B – Emission ScenarioA1B, described in Assessment Report 4 of IPCC

AR5 – IPCC Fifth Assessment Report

CanESM – Canadian GCM

CMIP5 – Coupled Model Inter-comparison Project Phase 5

CNE – Central North America

DSM – Downscaling method

ECCC – Environment and Climate Change Canada

ENE – Eastern North America

GCM – General Circulation Models

GHG – **G**reenhouse gas

GRL – **G**reenland

IDF – Intensity–Duration–Frequency

IPCC – Intergovernmental Panel on Climate Change

MOECC – Ontario Ministry of Environment and Climate Change

MPI-ESM-LR – GCM covered by CMIP5

MSC – Meteorological Service of Canada

MTO – Ontario Ministry of Transportation

OCCDP – Ontario Climate Change Data Portal

PCIC – Pacific Climate Impact Consortium

RCM – Regional Climate Model

RCP – Representative Concentration Pathways; 2.6, 4.5 and 8.5

RTA – Regional Trend Analysis

WATMAPPR – Waterloo Multiple Physiographic Parameter Regression

WIT3 – Waterloo Interpolator-Time, Topography, Temperature

Chapter 1: Introduction

1.1 State of Art:

An increase in extreme hydro-meteorological disasters such as hurricanes, typhoons, floods, and droughts, has led to devastating losses and suffering. The uncertainty of climate change, and the new extremes it brings, makes these challenges even more significant. Changes in climate conditions observed over the last decades are considered the cause of dramatic modifications in both the magnitude and frequency of the occurrence of extreme events (IPCC 2013). Changes in extreme rainfall events require new standards for infrastructure design and for the reconstruction and upgrade of existing infrastructure. Current design standards are based on historic climate information. A dam designed to control a 100 y flood event, by 1960 standards, provides a significantly lower level of protection if the intensity and duration of the 100 y flood event increases over the ensuing five decades. Incorporating the expected changes in planning and design of hydraulic structures will reduce unseen future uncertainties, (Srivastav, Schardong, & Simonovic, 2014).

Addressing the effects of climate change, and the development of disaster management plans, is a priority for many governments and institutions. Anthropogenic global climate change has stimulated considerable research focused on the prediction of climate scenarios, and its effect on Earth. An important aspect of these studies is the characterization of possible changes in climate extremes such as floods, droughts, and high winds.

Several studies explore the trends in heavy precipitation intensities in a global warming scenario. Historic records show an increase in heavy and very heavy precipitation intensities over the 20th Century in several regions of the world (Groisman *et al.*, 2005). A major part of the

available scenario simulations of future climate, using Global Circulation Models (GCMs) and Regional Climate Models (RCMs), show an increase in the heavier precipitation intensity and decreasing lighter precipitation (Allen and Ingram, 2002; Meehl *et al.*, 2005; Sun *et al.*, 2007). Possible processes that influence the increase in extreme precipitation intensities include changes in the atmospheric circulation (Emori and Brown, 2005; Berg *et al.*., 2009). Further influences include changes in the large-scale distribution of atmospheric aerosols and their effect on the distribution of energy in the troposphere and on the surface, and the intensification and invigoration of the cloud and precipitation formation process (Allen and Ingram 2002). For the latter of these processes, it is argued that a rise in surface temperature will enhance the intensity of heavy precipitation events through an increase in atmospheric moisture, which feeds a precipitation event through low-level moisture convergence (Trenberth *et al*., 2003). The Fifth Assessment Report (AR5) of the Intergovernmental Panel on Climate Change (IPCC) indicates a global surface temperature increase of 0.3 to 4.8 °C by the year 2100, compared to the reference period 1986–2005, with greater change in the Tropics and Subtropics than in the mid-altitudes. Researchers expect that rising temperatures will have a major impact on the magnitude and frequency of extreme precipitation events in some regions (Barnett *et al.*, 2006; Wilcox and Donner, 2007; Allan and Soden, 2008; Solaiman *et al.*, 2011). The hypothesis is that precipitation intensity will increase alongside atmospheric temperature due to the latter's greater capacity for moisture as temperatures rise.

Many researchers and practitioners focus on the potential change of frequency, intensity, and volume of extreme rainfall that climate change causes. Existing drainage systems are designed to the extremes that past records of rainfall events define, which in most cases makes them insufficient to accommodate future extremes. The development of appropriate present and

future Intensity–Duration–Frequency (IDF) curves helps address this, and assists in hydrological studies of urban drainage system performance analysis, design, and operation.

IDF curves describe the extreme rainfall patterns of a location. They define the probability that a storm of a given intensity and duration will occur in a given year. This probability is called a return period. Simply put, on average, a 2 y storm occurs every two years, a 5 y storm occurs once every five years, and so on. IDF curves summarize this annual probability of exceedance of storm intensity $P(R, \tau)$ given a storm's duration, τ (h). P is also known as the probability function. The return period, T, is defined by:

$$T = 1/P(R, \tau) \tag{1}$$

Equation (2) expresses the commonly assured relation between, rainfall intensity and duration for a given return period, T:

$$R = A\tau^B \tag{2}$$

where:

$$R = D/\tau \tag{3}$$

A = coefficient for rainfall intensity in mm/h that reflects the variation in location and return period,

B = dimensionless coefficient that reflects the variation in location and return period,

R = rainfall intensity (mm/h),

D = rainfall depth (mm),

τ = event duration (h), and

T = return period (y).

Equation 2 is also known as the IDF curve. The IDF curve power-law interpolates intensity values between the common durations of 5 min, 10 min, 15 min, 30 min, 60 min, 2 h, 6 h, 12 h, and 24 h. The Regional Trend Analysis (RTA) model uses the two-parameter, *AB* model, which is the same method that the Meteorological Service of Canada (MSC) uses for the calculation of IDF curves.

Figure 1 is an example of an IDF curve calculated for the St. Catharines A weather station in Ontario.

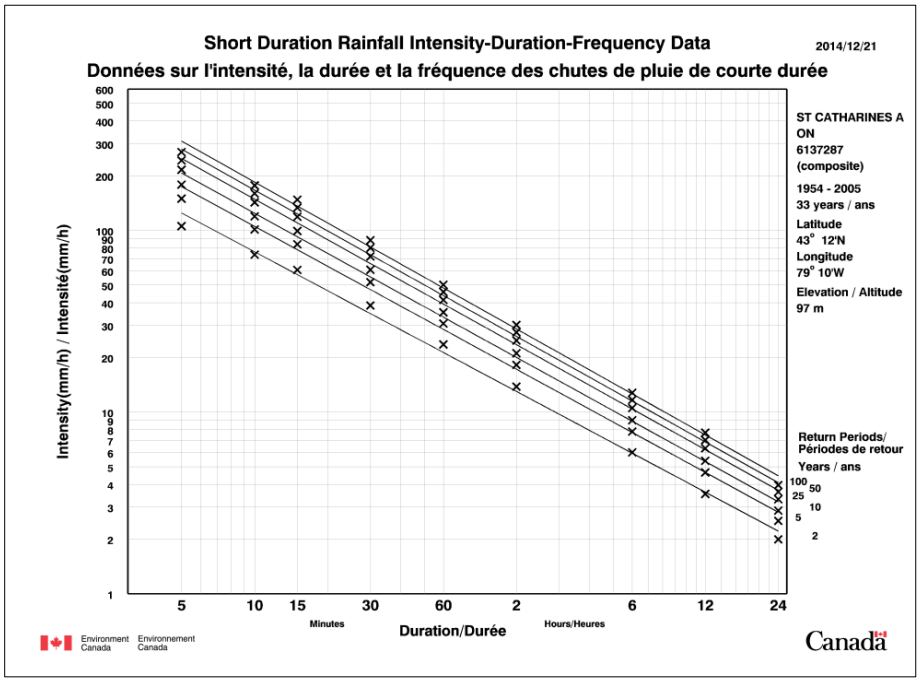

Figure 1: Sample MSC IDF curve for St. Catharines A (MSC 2014)

Hydrologic design of storm sewers, culverts, detention basins, and other elements of storm water management systems are typically performed based on specified design storms derived from the IDF curves (Solaiman and Simonovic, 2010). The main assumption in this process is that the historical series are stationary, and therefore can be used to represent the future extreme conditions. This assumption is questionable under rapidly changing conditions, and therefore IDF curves that rely only on the historical observations, will misrepresent future

conditions (Milly *et al.*, 2008). GCMs are one of the ways to explicitly incorporate changing, non-stationarity climate conditions for future periods.

1.2 Motivation:

Generally, GCM outputs are used for regional climate change impact assessments. GCMs provide temporal trends of global climate variables, such as sea level pressure, temperature, and specific humidity, based on different emission global scenarios of greenhouse gas (GHG) emissions. GCM outputs do not capture rapidly changing fields, such as precipitation. A combined examination of climate model simulations using GCMs based on multiple emission scenarios, and observation-based data sets, suggests more intense and frequent precipitation extremes under 21st-century warming scenarios. The intensifying trend of precipitation extremes has quantifiable impacts on IDF curves (Zhu, Forsee, Schumer, & Gautam, 2013; Kao and Ganguly 2011). Future research must improve regional estimates of precipitation extremes from higher resolution models, and locally develop regional- and local-scale IDF curves, which do not depend upon the stationarity assumption.

A preliminary analyses of high resolution datasets, such as the database from Pacific Climate Impact Consortium (PCIC) that is statistically downscaled to 10 km resolution, was performed for the historical period of 1960-2010. The empirical distribution of centered and time-adjusted PCIC data was plotted for 177 stations. The same was also done with MSC data. Figure 2 presents the comparison between the two. The PCIC data has a significantly lower standard deviation than that of the historical data, which results in upper quantiles (90 %, 95 %, etc.) that are lower than those of the observed historical data. This supports the claim that

precipitation forecasts based on downscaled climate scenarios are unsuitable for IDF curve forecasts, which is the basis for this research.

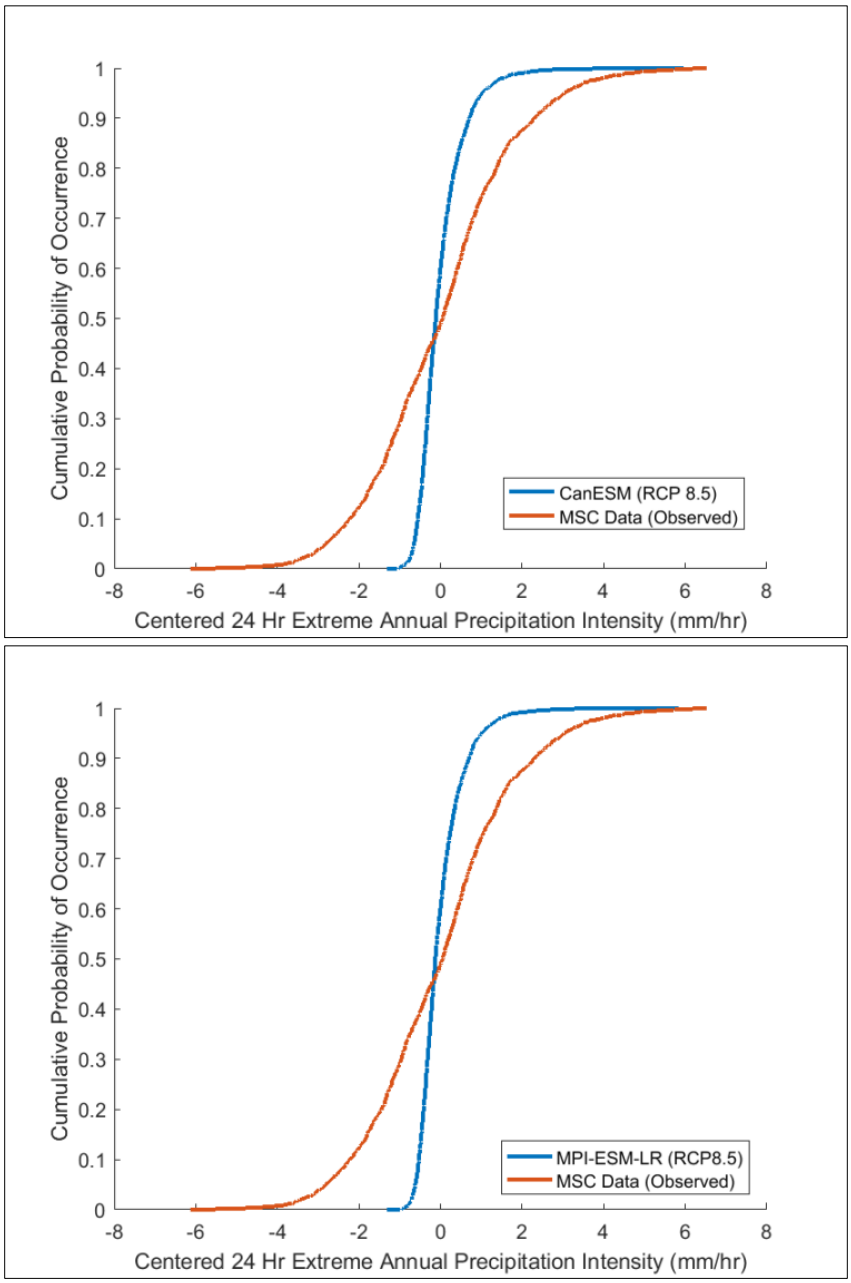

Figure 2: Probabilistic precipitation estimate comparison of PCIC data (blue) with historical MSC extreme precipitation data (red)

1.3 Objective:

As seen in previous section, precipitation forecast directly through downscaled GCMs are ineffective and are likely to lead to erroneous outcomes. Temperature predictions for future climate, on the other hand, are very good, as Chapter 4 details. An increase in global average temperature directly impacts precipitation because it drives evapotranspiration rates, and increases the concentration of water vapor in the atmosphere. With these facts in mind, this research develops an extreme precipitation forecast based on atmospheric thermodynamics, using future temperature forecasts. This study also combines already established regional temporal trends of precipitation with local topography. To prepare for future changes in the climate, and to avoid the dangers of under-designed infrastructure, we must review and update the current standards for water management infrastructure design. As climate change is dynamically changing the environment, so does the need of varying and nonstationary IDF curves. Thus, another objective of this research is to, refine IDF curves for Ontario. This may help, prevent water management infrastructure from performing below the designated guidelines in the future (Prodanovic and Simonovic, 2007). This study was funded by the Ontario Ministry of Environment and Climate Change (MOECC). Its main objective was to refine IDF curves, and come up with best possible probabilistic forecast of extreme precipitation for Ontario using temperature as a surrogate to hind-cast annual daily maximum precipitation for future years, and to evaluate the impact of climate change on IDF curves.

1.4 Organisation of Thesis:

The contents of this thesis are organized into the following chapters:

Chapter 2 provides a review of studies that posed the need of nonstationary design guidelines, in view of climate change, especially IDF values, while forecasting future extreme precipitation. The RTA approach which initiated nonstationary prediction of IDF curve is also discussed here. Brief overview is also done on precipitation and temperature relationship studies, especially the CCR and its application in forecasting extreme precipitation. This chapter also overviews GCMs, RCMs, and GHG emission scenarios.

Chapter 3 describes model database preparation and model development methodology.

Chapter 4 presents the model performance in comparison with existing models and also gives insight into future projections of extreme precipitation.

Chapter 5 identifies the risk and uncertainty areas pertaining to future predictions

Chapter 6 summarizes the results, and highlights some of the limitations and areas for future work.

Chpater 7 covers references.

Appendix-A briefly describes the application of WIT 3 predicted IDF values and extreme rainfall intensity.

Appendix-B shows sample nonstationary IDF curves developed for St. Catharines.

Chapter 2: Literature Review

2.1: Nonstationarity in the context of climate change:

Extreme climatic events are growing more severe and frequent. This observation calls into question how prepared our infrastructure is to deal with these changes. A precondition for traditional frequency analysis of precipitation is the assumption of stationarity. This assumption is that the controlling environmental factors, such as climate and land cover, act in the same way in the past, present and future (Gilroy and McCuen, 2012; Katz, 2013; Benyahya *et al*., 2014; Charles and Patrick, 2014). Studies show that, in some places, hydrological records exhibit some type of nonstationarity in the form of increasing or decreasing trends (e.g Olsen *et al.*, 1999; Strupzewski *et al.*, 2001; Sarhadi and Soulis, 2017; Douglas *et al.*, 2000; Lins and Slack, 1999). Anthropogenic activities, such as change in land use, urbanization, deforestation, and commercial agriculture are some of the leading causes of changes in the hydrologic cycle, affecting precipitation (Konrad and Booth, 2002; Villarini *et al*., 2009b; Hejazi and Markus, 2009; Vogel *et al.*, 2011; Pielke *et al.*, 2007). Some of the observed changes in hydrological records are from the effect of natural climatic variability. The variability results particularly from low-frequency components of climate variability such as the El Niño Southern Oscillation (ENSO), and decadal and multi decadal oscillations such as the Pacific Decadal Oscillation (PDO) and the Atlantic Multidecadal Oscillation (AMO). These large-scale forcing exert in-phase and out-of-phase oscillations in the magnitude of hydrologic events such as extreme precipitation, extreme floods, droughts, and extreme sea levels (e.g., Mantua *et al.*, 1997; Jain and Lall, 2000, 2001; Enfield *et al.*, 2001; McCabe and Wolock, 2002; Franks and Kuczera, 2002; Keim *et al.*, 2003; Park *et al.*, 2010, 2011).

The concept of nonstationarity is also important in the context of climate change, due to ascending levels of GHGs in the atmosphere. Studies (IPCC 2013) are pinpointing towards change in the recurrence interval, severity, and spatial coverage of extreme events, under elevated levels of temperature. Event return period, or recurrence interval, and the associated risk of occurrence are also critical considerations in the management of water resources, especially regarding design and operation of hydraulic structures. To tackle non-stationarity of hydrologic extremes, several approaches have been proposed in the literature, such as frequency analysis methods, in which the parameters (or moments such as the mean and variance) of a given distribution (e.g., the Gumbel) may vary in accordance with time (Soulis et al., 2016).

One approach of handling nonstationarity is using probability distributions with temporal trend to identify changes in parameters, or mean variance (Strupczewski *et al.*. 2001; El Adlouni *et al*., 2007; Cooley, 2013; Katz, 2013; Sarhadi and Soulis, 2017). Another approach uses stochastic models with shifting patterns (Sveinsson *et al.*, 2005). Finally, some models have also used covariates (Katz *et al.*, 2002; Griffis and Stedinger, 2007).

This research uses the RTA method, established by Soulis *et al.* (2016) , which uses local topography as independent variables to establish temporal trends for extreme precipitation. Soulis *et al*. (2016) carried out the time trend analysis using observations from 1960 to 2014. A linear trend was observed and extrapolated from this period to 2060. The analysis combined the datasets from all stations and determines their collective historical trend. The projections were extrapolations based on historical trends and assumed that the rate of change, m, will stay constant.

The formula for future IDF curve intensities, Rt' for year $t' > 2010$, uses the following equation:

$$R_{t'} = A_{2010} \cdot \tau^B + m \cdot (t' - 2010) \quad (4)$$

There are seven independent variables (longitude, latitude, barrier height to west, slope in east-west direction, slope in north-south direction, proximity to water, and elevation) for which multiple linear regressions are performed using the equation below.

$$\overrightarrow{Y} = X\vec{\beta} + \vec{\varepsilon} \quad (5)$$

Here, $\vec{Y}$ is the natural log of A parameters generated from the regression analysis, X is the matrix of the independent physiographic characteristics, $\vec{\beta}$ is the partial regression coefficient vector, and lastly $\vec{\varepsilon}$ is the error vector from the analysis.

With least squares fit, $\vec{\beta}$ is found with:

$$\vec{\beta} = (X^T X)^{-1} X^T \vec{Y} \quad (6)$$

The normalized error, ε, for the mean response is derived with the following formulas:

$$\varepsilon_1 = SE_1 \cdot \tau^B \sqrt{1 + \frac{1}{n_1}} \quad (7)$$

$$\varepsilon_2 = SE_2 \cdot \sqrt{\frac{1}{n_2} \left(1 + \frac{(2010 - \bar{t})^2}{\sigma_t^2}\right)} \quad (8)$$

$$\varepsilon = \sqrt{\varepsilon_1^2 + \varepsilon_2^2} \quad (9)$$

in which, SE_1 is the root-mean-square deviation of the residuals from the regression of A parameters against physiographic characteristics, SE_2 is the rate of change of the rainfall rate per year, and $\bar{t}$ is the mean calendar year in the dataset for each storm duration.

Temporal variation in the precipitation intensity was observed, and based on that, linear regional precipitation trend was identified by Soulis et.al. (2016). This is the first step, and evidence from Sarhadi and Soulis (2017) exemplified that, time is major driving factor in future precipitation forecast, not necessarily linear. Therefore, results in the study are adequate for interpolation in time and should be used with caution, for extrapolation.

Upcoming chapters show, how extreme precipitation values, are sensitive to elevated temperatures and other climate change effects using climate scenarios.

2.2: Relationship between temperature and precipitation:

The CCR states that the saturation partial pressure of water vapor increases with exponential function of temperature. The observed water vapor content of the atmosphere, also follows this approximate exponential relation with respect to surface temperature (Stephens 1990). The CCR also predicts the partial pressure increases at a rate of about 6% K^{-1} at 300 K and 15% K^{-1} at 200 K.

Trenberth *et al.* (2003) found a fractional rate of increase in saturation specific humidity of ~7% K^{-1} to be representative based on consideration of the CCR and global-mean temperatures at pressures of 700 and 850 hPa. Similarly, column water vapor varies with surface temperature at a rate of ~9% K^{-1} in observations over tropical oceans. This relates to CCR scaling, assumes a constant rate of change with respect to a lower-tropospheric temperature, and relates the lower-tropospheric and surface temperature variations using a constant factor related to the moist-adiabatic lapse rate (Wentz and Schabel, 2000).

Increases in the amount of atmospheric water vapor under global warming are of climatic importance because of water vapor's role in energy transport by latent heat fluxes, patterns of

precipitation and evaporation, radiative transfer, and freshwater exchange with the ocean (Peixoto and Oort, 1992). The increase in the amount of water vapor for a given temperature change is strongly constrained by the CCR. This gives a fractional rate of change of saturation vapor pressure that varies substantially over the range of typical tropospheric temperatures from ∼6% K^{-1} at 300 K to ∼15% K^{-1} at 200 K. It is also believed that increased capacity of water vapor at given temperature, results in short term extreme rainfall and ultimately flash flooding.

Studies show that, it is difficult to predict rainfall and temperature at a time, as a strong correlation exist between them (Shukla and Mishra, 1977; Moise *et al.*, 2012; Tanarhte *et al.*, 2012). Aldrian and Dwi Susanto (2003), confirmed the sensitivity of Indonesian rainfall variability with sea-surface temperature variability. Black (2005), associated east Africa rainfall with Indian Ocean surface temperature, while Rajeevan *et al.* (1998), and Huang *et al.* (2009) found a negative correlation between rainfall and temperature.

The preliminary analysis for this study found that precipitation changes with change in temperature. This study uses saturated vapor pressure, computed based on CCR, which is computed from annual maximum temperature. The basic assumption made over here is, saturated vapour pressure is indirectly related with, extreme precipitation.

2.3 Overview of General Circulation Models (GCMs), Downscaling Methods (DSMs), and Emission Scenarios (RCPs)

The IPCC defined GCMs as numerical models that represent physical processes in the atmosphere, ocean, cryosphere, and land surface. These are the most advanced tools currently available (IPCC 2013) for simulating the response of the global climate system to increasing GHG concentrations.

The GCMs simulate the atmospheric patterns on larger grid scales (>100 km), whereas, regional climate models (RCM) are developed to incorporate the local-scale effects and have smaller grid scales (25 to 50 km). Both GCM and RCM models, however, have large grid scales when compared to the size of most watersheds. Downscaling is one of the techniques to link these GCM and RCM grid scales with the local study areas. These are broadly classified into dynamic downscaling and statistical downscaling. The dynamic downscaling procedure uses higher resolution GCMs to simulate the local conditions (Mandal *et al.*, 2016), whereas the statistical downscaling procedure is based on transfer functions which relate the GCMs with local study areas (Li *et al.*, 2010). Statistical downscaling procedures are widely used when compared to the dynamic models because of their lower computational requirements and availability of outputs for a wider range of emission scenarios.

A number of studies uses, station downscaled GCMs or RCMs to update the IDF curves (Mailhot *et al.*, 2007; Nguyen *et al.*, 2007; Solaiman and Simonovic, 2011; Kao and Ganguly, 2011; Peck *et al.*, 2012; Mirhosseini *et al.*, 2013; Hassanzadeh *et al.*, 2013). However, GCMs contain biases relative to observed data because of their parameterization systems and large grid size. At the regional scale, this is sometimes acceptable, but not at the basin scale.

The IPCC generated Assessment Report 5 (AR5) is based on the Coupled Model Inter-Comparison Project Phase 5 (CMIP5) ensemble projections, which are quality-checked data. CMIP5 make use of Representative Concentration Pathways (RCPs), which are designed to provide plausible future scenarios (IPCC, 2013) of anthropogenic forcing spanning a range from a low emission scenario, characterized by active mitigation (RCP 2.6), through two immediate scenarios (RCP 4.5 and 6.0), to a high emission scenario (RCP 8.5). Each RCP is associated with plausible combinations of projected population growth, economic activity, energy intensity, and

socio-economic development. The RCP scenarios were named based on their total radiative forcing by 2100.

RCP 2.6 represents a peak in net radiative forcing at approximately 3W/m^2 by mid-century, before declining to 2.6 W/m^2 by 2100. RCP 4.5 and 6.0 represent stabilization (without overshoot) in net radiative forcing at 4.5 W/m^2 and 6.0 W/m^2 post-2100. RCP 8.5 represents a rise in radiative forcing to 8.5 W/m^2 in 2100.

These RCP scenarios serves as input to Earth System Models (ESMs), which simulate the climate system response and resulting conditions (IPCC 2013). In this study, two GCMs (CanESM 4.2 and MPIESM) and three RCP scenarios (RCP 2.6, 4.5, and 8.5) are considered. The following chapter describes the factors, database, and methodology used to develop the model.

Chapter 3: Methodology

3.1 Model Database Preparation:

3.1.1 Local topography data:

The physiographic parameters that this study uses are adopted from the RTA developed by Soulis *et al.* in 2016. The RTA uses seven parameters as predictors of IDF curve values. This method is based on Waterloo Multiple Physiographic Parameter Regression (WATMAPPR). (Seglenieks, 2009). RTA establishes a linear regional temporal trend for annual daily maximum precipitation, and enables the prediction of nonstationary IDF curve values for Ontario.

The WATMAPPR technique uses these seven physiographic parameters:

- Elevation – The average elevation of the grid square(m).
- Latitude – The latitude of the grid square (degree).
- Longitude – The longitude of the grid square(degree).
- East/west slope – The difference in elevation between the grid squares on either side of the station grid square, divided by the horizontal distance between the grid squares in both the east/west direction.
- North/south slope – The same as the east/west slope, but in a north/south orientation.
- Distance to water – the distance between that point and closest large body of water (i.e. Hudson Bay, or one of the Great Lakes including Georgian Bay, but not Lake Nipigon, Lake Nipissing, or Lake Simcoe) (m).
- Barrier height to the west - The difference between the elevation of the grid square and the highest elevation towards the west, reset at large bodies of water (m).

3.1.2 Precipitation:

The station data for this study come from the Environment Canada National Climate Data Information Archive (MSC, 2014). The data set includes 147 stations from Ontario, of which only 133 are used in this study, while the remaining stations were removed as outliers because they were outside the 95% confidence limits. The MSC stations have the greatest concentrations in Southern Ontario. For the 133 stations used, the record lengths vary from 5 years to 53 years, with an average record length of 26 years. Only station records from 1960 and later are used, with 2013 as the final year as it is the most recent year with published data.

3.1.3 Temperature:

The daily maximum, minimum, and mean temperature values are from Environment and Climate Change Canada's (ECCC) Historical Climate Data in the National Climate Data Information Archive. Of 133 stations across Ontario, 22 are not used as their temperature and precipitation data values do not temporally overlap with each other. The remaining 111 stations have temporally overlapped precipitation and temperature values. They are analyzed with the statistics program, R, to filter out annual maximum and mean temperature values.

ECCC divides the temperature database into three categories: minimum, mean, and extreme daily temperature. For this study, only mean daily temperature is considered representative. Mean daily temperature values are first used to determine monthly maximum values. The highest value in that 12-month set was chosen as the annual daily maximum temperature for a station for that calendar year.

To determine the annual mean temperature, daily mean values are averaged for each month. This yields the monthly mean temperature value. The average of the 12-month mean

temperature values for a given year is termed as annual mean temperature. For simplicity, the annual mean temperature is referred to simply as the mean for the remainder of this thesis.

Annual daily maximum temperature values, were used to compute annual maximum saturated vapour pressure using following relationship (Dingman, 2002):

$$e^* = 0.611 \cdot exp(\frac{17.3 \cdot \theta}{\theta + 237.3}) \quad (10)$$

where:

θ = annual daily maximum temperature (°C), and

e^* = saturated vapour pressure (kPa).

3.2: Model Development

The physiographic parameters from section *3.1.1*, are supplemented with saturated vapour pressure, annual mean temperature values, and time anomaly ([*year*] – [*base year*]; where *base year* = 2010), for a total of ten independent variables. Multiple linear regressions are performed, using annual daily maximum rainfall intensity as the dependent variable.

A backward selection procedure was implemented to select an optimal linear model first by eliminating insignificant model terms. In each iteration of the selection procedure, the p-values of the various parameters are examined, and the parameter with the largest p-value (lowest significance) is dropped from the model. This process was repeated until no parameters remain with p-values greater than 0.05.

Two exceptions are made to this procedure. The mean temperature was kept as a predictor, despite being slightly above the p-value threshold, since temperature increases the model's nonstationary potential. Temperature, unlike the other physiographic variables, is also tied to climate change, so it has the greatest potential as a predictor. The second exception to the

procedure is the selection of barrier height to the west as a predictor, rather than distance to water, despite a slightly higher p-value. Barrier height to the west, relative to distance to water, has a weaker correlation with the other variables, and thus has greater use in the spatial interpolation.

The result is an expression that relates the value of the maximum precipitation with time, annual mean temperature, saturated vapour pressure, barrier height to the west, and latitude/longitude, for any location in Ontario. This equation calculates the expected value of the daily maximum precipitation for a given calendar year at respective stations in Ontario. Table 1 shows values and statistics of the model coefficients. The standard error of the model is 0.786.

Table 1: Model Statistics

	Coefficients	**Standard error**	**t-stat**	**P-value**
Intercept	2.270	0.631	3.600	0.000325
Year-2010 (Δt)	0.00551	0.00147	3.760	0.000175
Mean temperature ($\bar{\theta}$)	0.0260	0.0135	1.922	0.0547
Saturated vapour pressure (e^*)	-0.0705	0.0316	-2.231	0.0258
Longitude (I_1)	-0.0139	0.00612	-2.268	0.0234
Latitude (I_2)	-0.0279	0.0123	-2.274	0.0231
Barrier height to west (I_3)	-0.000819	0.000401	-2.044	0.0411

The final equation is:

$$R_n(t|\tau = 24) = B_0 + B_1 \cdot \Delta t + B_2 \cdot \bar{\theta}(\mathrm{t}) + B_3 \cdot e^*(\mathrm{t}) + B_4 \cdot I_1 + B_5 \cdot I_2 + B_6 \cdot I_3 + \varepsilon \quad (11)$$

where:

$R_n(t|\tau = 24)$ = 24 h rainfall intensity in year *t* (mm/h),

B_0 = intercept,

$B_1, B_2, B_3, B_4, B_5, B_6$ = coefficients,

Δt = Time anomaly $(t - t_0)$ (y),

$\bar{\theta}(t)$ = mean temperature in year *t* (°C),

I_1 = longitude (decimal degree),

I_2 = latitude (decimal degree),

I_3 = barrier height to west (m),

$e^*(t)$ = saturated vapour pressure in year *t* (kPa),

t_0 = base year, 2010,

n = station ID, and

ε = random component (reflected in the residuals of the regression)

An analysis of the residuals revealed that, they follow a Gumbel distribution, as shown in Figure 3.

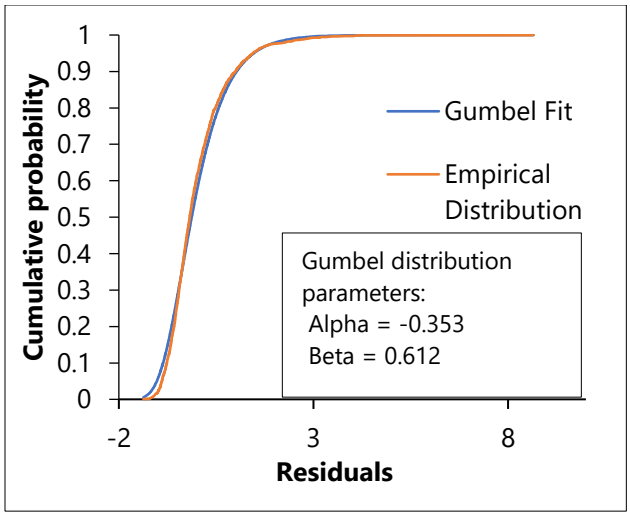

Figure 3: Residual analysis

In the classical stationary IDF curve analysis, Hogg *et al.*, (1989) use the following equation for each duration to determine station quantiles:

$$R_n(T,\tau) = \overline{R_n(\tau)} + K(T)S_n(\tau) \tag{12}$$

where:

$R_n(T,\tau)$ = storm intensity for the station,

$\overline{R_n(\tau)}$ = long-term average extreme rainfall,

$K(T)$ = Gumbel frequency factor for the return period,

$S_n(\tau)$ = long-term standard deviation of the extreme rainfall for the period of record,

T = return period,

τ = duration, and

n = station identification.

Soulis *et al.*, (2016) use Equation (12), to estimate $R_n(T,\tau)$, which varies yearly. Thus, in nonstationary form, Equation (13) gives the design rainfall intensity for a given return period and year.

$$R_n(T,t,\tau) = \overline{R_n(t,\tau)} + K(T)S_n(\tau) \quad (13)$$

where $\overline{Rn(t,\tau)}$ is the expected value from the precipitation-temperature model (Equation 11) for station n and year t.

Thus, the final equation, which estimates the design rainfall intensity of a 24 h storm for a given return period is:

$$R_n(T,t|\tau=24) = (B_0 + B_1 \cdot \Delta t + B_2 \cdot \bar{\theta}(t) + B_3 \cdot e^*(t) + B_4 \cdot I_1 + B_5 \cdot I_2 + B_6 \cdot I_3) + K(T) \cdot S_n \quad (14)$$

where:

$R(T,t|\tau=24)$ = estimated 24 h rainfall intensity for station n in year t for given return period,

B_0 = intercept,

$B_1, B_2, B_3, B_4, B_5, B_6$ = coefficients,

Δt = $(t - t_0)$ (y),

$\bar{\theta}(t)$ = mean temperature in year *t* (°C),

I_1 = longitude (decimal degree),

I_2 = latitude (decimal degree),

I_3 = barrier height to west (m),

$e^*(t)$ = saturated vapour pressure in year *t* (kPa),

$K(T)$ = Gumbel frequency factor for the return period,

n = station ID,

T = return period (y), and

S_n = residual standard error of the linear regression.

The difference between Equation 11 and Equation 14 is that ε is replaced by $K(T) \cdot S_n$. To calculate return period rainfall intensities for durations other than 24 h, Equation 2 can be rearranged into the following form:

$$R_n(T, t, \tau) = e^{ln[R_n(T,t|\tau=24)]+B(ln\,\tau - ln\,24)} \quad (15)$$

where:

$R_n(T, t, \tau = 24)$ = 24 h storm intensity for a given year and return period

B = slope of the IDF curve, generally equal to -0.699

τ = storm duration

This model is named as Waterloo Interpolator-Time, Topography, Temperature (WIT3). WIT3 has advantage of being nonstationary, in its dependence upon GCM-predicted temperature θ, and e^*_{sat} ,which makes it sensitive to varying climate change conditions, covering temperature effects and accommodating the regional temporal trend, established using RTA (Soulis *et al.*, 2016). The following chapter evaluates, efficiency of WIT3 in predicting Annual Maximum Precipitation (AMP) for historical period 1960-2010, by comparing it with, actual observations (MSC) and predictions by other stationary and nonstationary methods. The chapter also covers probable estimates of precipitation intensities for future years across Ontario.

Chapter 4: Model Performance Comparison and Future Projections

4.1: Model Performance Comparison

This study compares WIT3 with two other models (tools), along with the actual annual daily maximum precipitation observations from MSC. The RTA model is sensitive to local topography, and establishes linear temporal trends of annual maximum precipitation. Thus, it is nonstationary and sensitive enough to accommodate local physiography, and orographic effect. The same is already used by the Ontario Ministry of Transportation (MTO) via its online IDF Look-up Tool. Another is the GCM-based model that the Ontario Climate Change Data Portal (OCCDP) uses. The additional advantage of the OCCDP model is its use of GCMs, which account for future demography, radiation, land use pattern, GHG emission levels, and several other factors, to replicate climate change. Unfortunately, the OCCDP is not bias-corrected. WIT3 combines the benefits of both models, and combines local topography and temporal trends along with accommodations of GCMs and three GHG emission scenarios. WIT3 has an added advantage in that, it considers temperature and resulting atmospheric thermodynamics. The following section compares the three methods.

4.1.1: Database Selection for Comparison and Results:

The WIT3 model uses the historic relationship between temperature and precipitation in Ontario to refine extreme precipitation projections. For the historical comparison, 56 stations were selected that have a minimum of 20 years of records in total. The stations were also required to have historic temperature and precipitation records that overlap each other by 10 or more years. The average record year for each station was then identified.

4.1.1: Model Outcome and Comparison:

The results from WIT3 and the RTA model were then time corrected to each station's average years for accurate comparisons alongside the each other and the OCCDP data. Figure 4 shows the geographic distribution of eight stations selected from across Ontario for the comparison of extreme rainfall intensity with corresponding return periods, while Figure 5 shows the results. Note that, due to the nature of the data available for the OCCDP, those results cannot be time-adjusted, as they are given as a stationary value for the years 1960 to 1990.

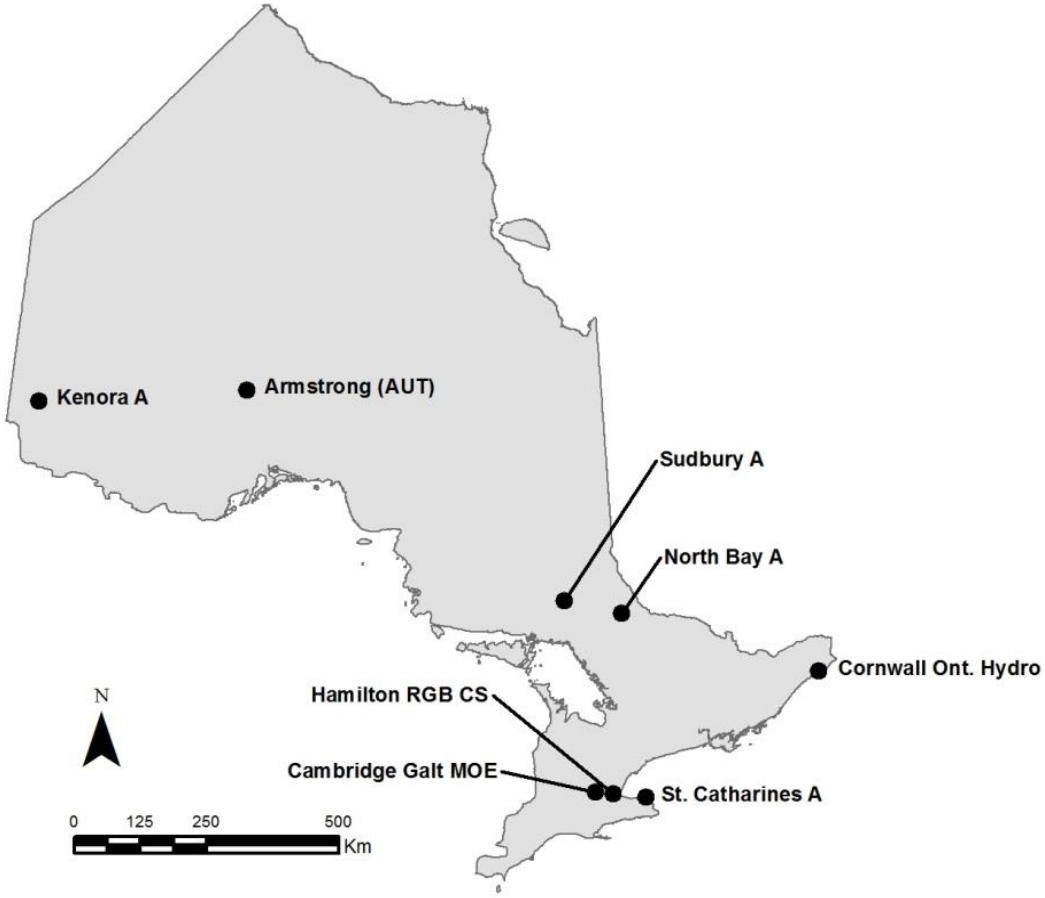

Figure 4: Geographic distribution of sample stations

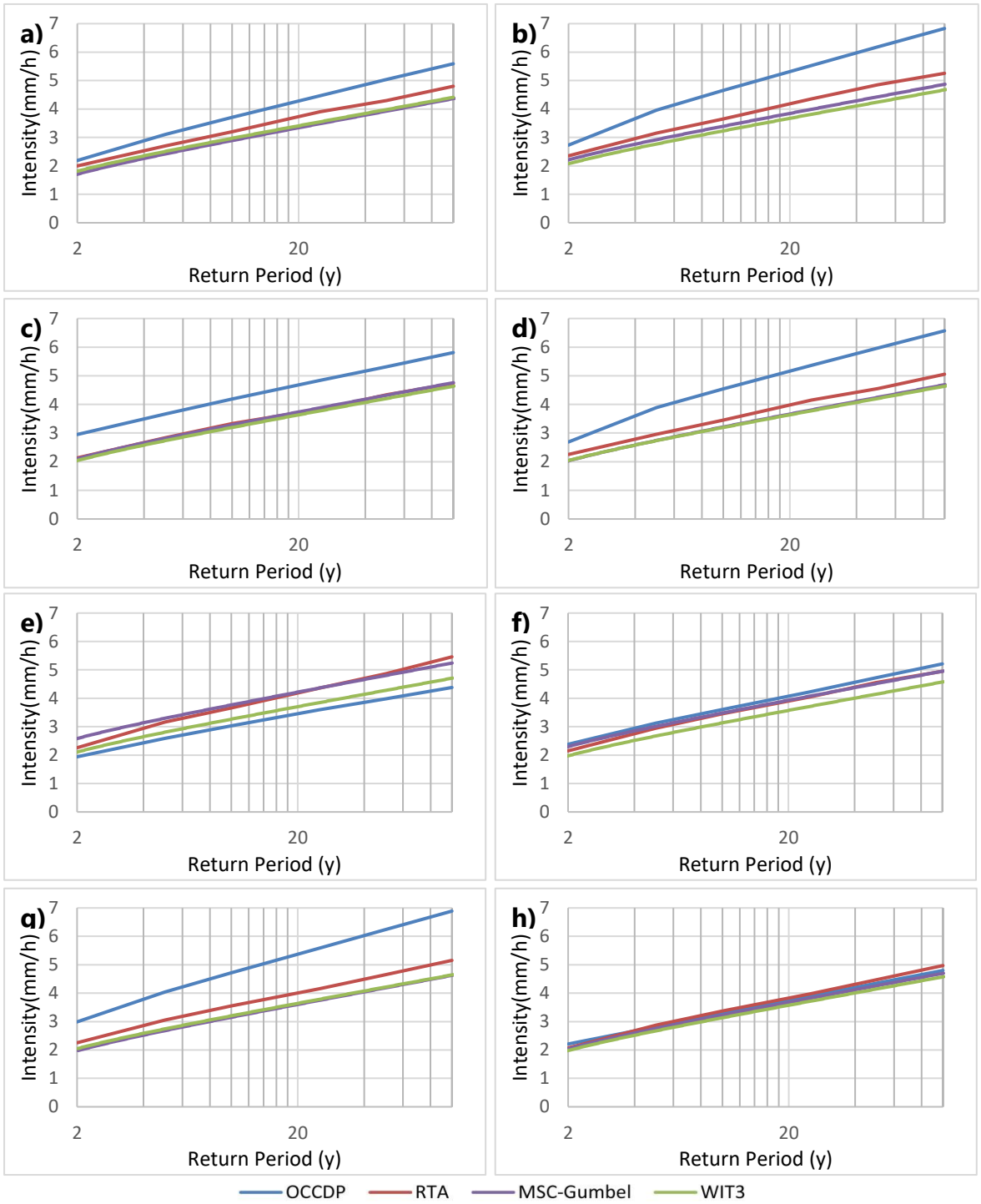

Figure 5: Comparison of 24 h rainfall intensity return period estimates for eight stations across Ontario for period, 1960-2010 for a) Armstrong, b) Cambridge Galt MOE, c) Cornwall, d) Hamilton RBG CS, e) Kenora A, f) North Bay, g) St. Catharines A, and h) Sudbury A

Model quantiles were compared to the quantiles of the Gumbel-fitted MSC data, which was selected as the best estimate of the true distribution of actual station data. This is a Gumbel distribution, which has been parameterized for each station using the station mean and the standard deviation of the overall MSC dataset. This overall standard deviation was used under the assumption of a constant standard deviation across Ontario.

The same procedure was carried out for the remaining 48 stations, for a total of 56. The comparison was made on the 2, 5, 10, 25, 50 and 100 y return period rainfall intensity values for the 24 h storm. Figure 6 presents the statistics on the differences (deltas) in these return period values, in mm/h, between the MSC Gumbel and the three models. Figure 6 (a) to (c) shows the difference between the MSC Gumbel and modeled results for the 24 h annual maximum rainfall intensity at the 99^{th} percentile (100 y return period). Since, for ease of communication, the scales are not consistent between comparisons, the histogram in Figure 6 (d) illustrates the distribution of the deltas on a common scale.

As the histogram shows, the WIT3 model has the largest number of observations near zero. This indicates that the WIT3 model represents the historical data with the least discrepancy between actual observations and WIT3 generated model output. Although the WIT3 quantiles tend to slightly underestimate those of the MSC Gumbel for higher return period values, as Figure 6 shows, the difference is negligible.

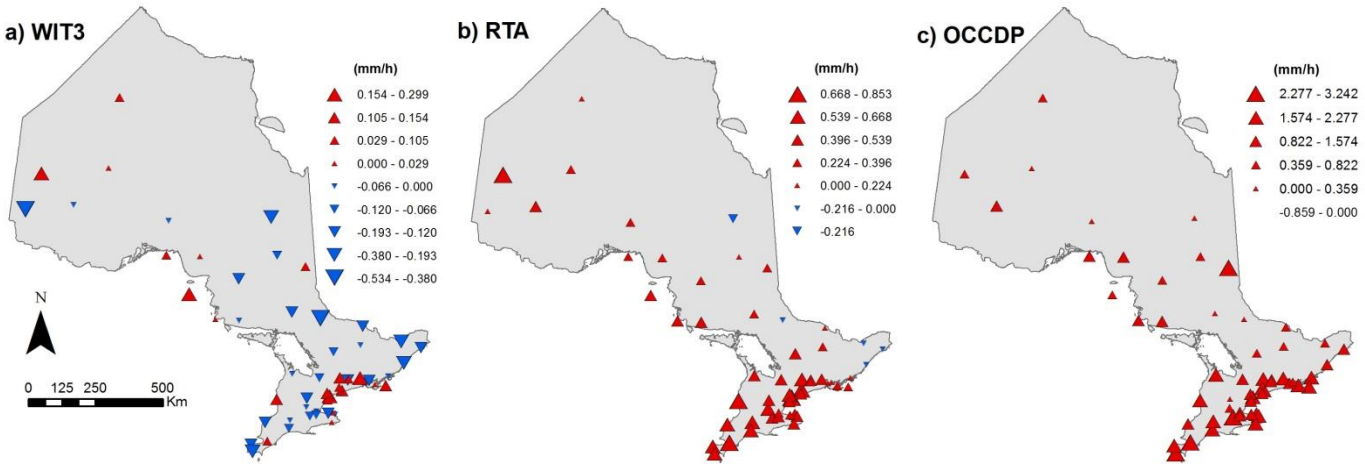

d) Distribution of the deltas on a single scale

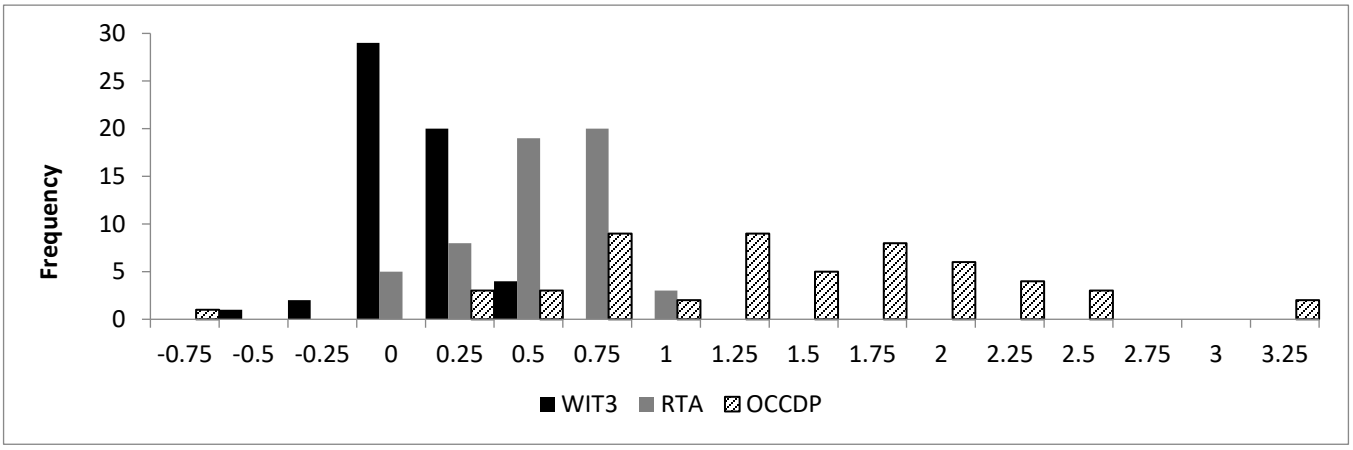

Figure 6: The difference in time-corrected rainfall intensity for the 100 y rainfall (99th percentile) between the empirical MSC data and results from a) the WIT3 model, b) the RTA model, and c) the OCCDP model. A histogram d) the distribution of the deltas

The RTA quantiles were also found to match those of the MSC Gumbel quite closely, but show potential for refinement as they, on average, tend to overestimate the historical quantiles. The OCCDP values, which represent the median IDF curve estimate from the AR4:A1B scenario, generally significantly overestimate the historical quantiles.

When compared, the WIT3 model has the closest match with the quantiles of historic data, and is therefore assumed to have the most accurate representation of future extreme precipitation scenarios. From Figure 4, Figure 5, and Table 2 one sees that the RTA predictions are better than OCCDP predictions, but looks slightly conservative, as compared to WIT3, which is extension of RTA.

Table 2: Mean differences between empirical MSC results and the modeled results for the 24 h storm, compared over 56 Ontario MSC station locations.

	Mean difference from MSC			Standard deviation of difference from MSC		
Return period (y)	**WIT3**	**RTA**	**OCCDP**	**WIT3**	**RTA**	**OCCDP**
2	0.03	0.20	0.58	0.15	0.37	0.37
5	0.01	0.26	0.77	0.15	0.47	0.47
10	0.00	0.30	0.89	0.15	0.53	0.53
25	-0.01	0.34	1.05	0.15	0.62	0.62
50	-0.02	0.37	1.17	0.15	0.69	0.69
100	-0.03	0.40	1.29	0.15	0.76	0.76

4.2 Future Projections Comparison:

To project the expected value of precipitation for future events, and using the year 2010 as a base, the input parameters required were annual daily maximum temperature and annual mean temperature. Various options were considered for future temperature data, such as GCM-based outputs, RCM-based temperature data, and different ensemble based temperature data. GCM

output is coarse as it has large gridded climate data, and needs to be downscaled using either dynamic or statistical methods for its output to be used in the temperature-precipitation model. Downscaling methods have different biases that affect the end data. RCM outputs are finer than GCM outputs, which mean their grid sizes are much smaller than GCM outputs, but RCM methods also have biases that affect output. Often, an ensemble approach is adopted to compensate for these different biases and to compensate for systematic errors. The IPCC used an ensemble approach to develop the best possible climate impact studies for future years. The IPCC's AR5, released in 2014, uses the data from CMIP5 that was also released in 2014. CMIP5 is the source of a quality assessed, reliable database used for scientific studies.

This study uses two sources for temperature inputs for future years: Ontario Climate Change Data Portal (OCCDP) and PCIC. OCCDP uses the Providing Regional Climate for Impact Studies (PRECIS) model, under the A1B emissions scenario and the RCM, under the RCP 8.5 emissions scenario. For this study, PRECIS data was selected for analysis. PRECIS is an ensemble of five GCMs, developed by the Hadley Centre for Meteorological Studies, in the United Kingdom. The GCMs use the A1B climate change scenario for future projections. The output from the OCCDP is downscaled to a 25 km resolution without bias correction, and is not continuous. The output is grouped into the 30 y periods of 1960-1990, 2015-2045, 2035-2065, and 2065-2095. PCIC output is historical daily gridded climate data based on an ensemble of 12 GCMs. PCIC contains historical data as well as future projections based on the IPCC's RCP 2.6, 4.5 and 8.5. The data are quality checked as they are based on CMIP5. The data are bias corrected and statistically downscaled to a 10 km resolution using two methods: Bias Correction Spatial Disaggregation (BCSD), and Bias Correction/Constructed Analogues with Quantile

mapping reordering (BCCAQ). BCCAQ is a hybrid method that combines results from BCCA (Maurer *et al.*, 2010) and quantile mapping (QMAP) (Gudmundsson *et al.*, 2012).

Observed historical data from ten randomly selected Environment Canada stations were used to compare the historical maximum temperature data from OCCDP and PCIC outputs from 1960-1990. Figure 7 shows the output for two stations, Hamilton and Kenora. The comparison of these ten sites revealed that PCIC data more closely matches the historical observed data. This is likely because the projections under AR4 at OCCDP were not bias-corrected.

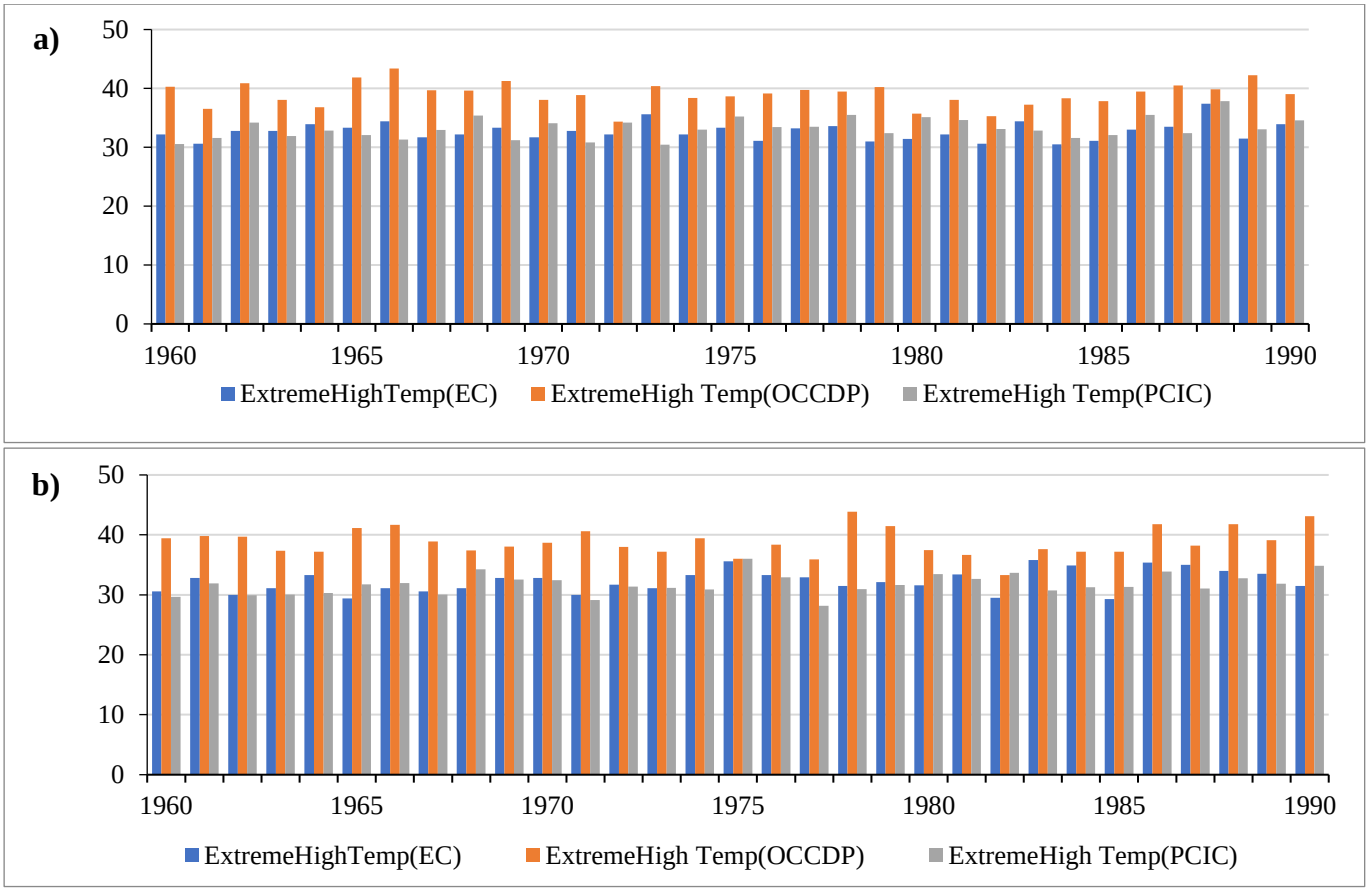

Figure 7: MSC (EC), OCCDP and PCIC extreme temperature comparisons for a) Hamilton, Ontario, and b) Kenora, Ontario.

Figure 8: Empirical distribution function for historical extreme temperature and MPI-ESM-LR-RCP 8.5 standardized by station mean, 1960-2010.

Figure 8 shows the results of an empirical distribution fitting exercise performed on observed data and PCIC data from 1960-2010. As in Figure 8, the data for each station were adjusted to equivalent 2010 values with a fitted linear trendline, and subsequently standardized by subtracting the station mean. This exercise revealed that the PCIC temperature database matches the distribution of observed data. It was determined that downscaled GCM temperature projections from the PCIC database are suitable for use as input into a precipitation forecast model. As discussed above, PCIC uses an ensemble of 12 GCMs. The authors adopted Cannon's (2015) approach, a method that orders GCM scenarios to provide the widest spread of projected climate scenarios for smaller subsets of the full ensemble. Table 3 shows the top five GCMs by region.

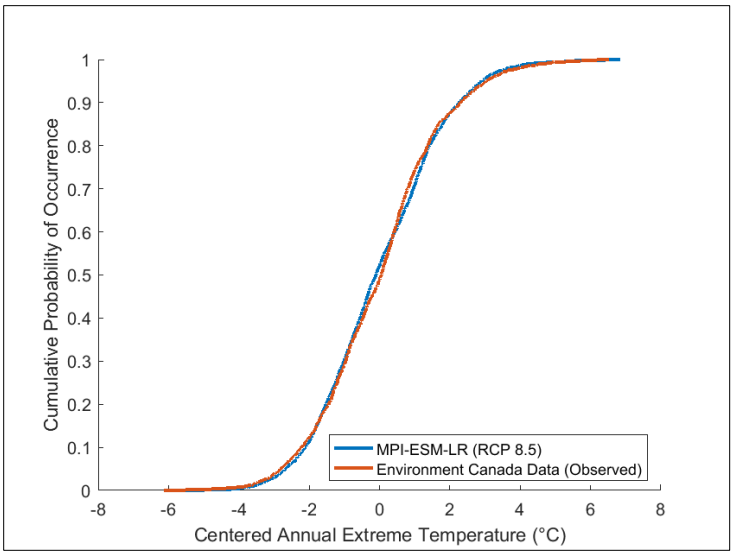

Figure 8: Empirical distribution function for historical extreme temperature and MPI-ESM-LR-RCP 8.5 standardized by station mean, 1960-2010.

Table 3: Model ensembles and Giorgi-Francisco regions

Order	Western North America (WNA)	Alaska (ALA)	Central North America (CAN)	Eastern North America (ENA)	Greenland (GRL)
1	CNRM-CM5-r1	CSIRO-Mk3-6-0-r1	CanESM2-r1	MPI-ESM-LR-r3	MPI-ESM-LR-r3
2	CanESM2-r1	HadGEM2-ES-r1	ACCESS1-0-r1	INMCM 4-r1	INMCM 4-r1
3	ACCESS1-0-r1	INMCM 4-r1	INMCM 4-r1	CNRM-CM5-r1	CanESM2-r1
4	INMCM4-r1	CanESM2-r1	CSIRO-Mk3-6-0-r1	CSIRO-Mk3-6-0-r1	CNRM-CM5-r1
5	CSIRO-Mk3-6-0-r1	ACCESS1-0-r1	MIROC5-r3	HadGEM2-ES-r1	ACCESS1-0-r1

As Giorgi and Francisco (2000) define, Ontario falls into three subcontinental regions: Central North America (CNA), Greenland (GRL), and Eastern North America (ENA). The top models for Ontario were CanESM and MPI-ESM. Consequently, downscaled temperature projections were downloaded for both GCMs. Each GCM output had three RCPs to choose from: RCP 2.6, RCP 4.5, and RCP 8.5. The author downloaded all three RCPs for both GCMs, resulting in a total of six climate scenarios. The temperature values were used as input into Equation (14), as described in Chapter 3, to generate extreme precipitation values. Equation (15) was then used to determine the corresponding return period rainfall intensity for arbitrary storm durations.

Starting with base year 2010, future 1 h, and 24 h rainfall intensity projections were made for years 2060 and 2090, using both the RTA and WIT3 models. The RTA model was based on the temporal variation of extreme precipitation with consideration of physiographic factors, while the WIT3 model forecasts extreme precipitation based on physiography, temperature, and time. Figure 9 and Figure 10 show the difference between the 100 y return period rainfall intensity values for the 1 h and 24 h storms, as predicted by WIT3 and RTA, for two GCMs: CanESM and

MPI-ESM. The RCP 8.5 scenario was chosen for comparison, as this is the most severe climate change scenario considered in this study.

Table 4 presents statistics on the difference in 1 h and 24 h extreme precipitation projections between RTA and WIT3 models for 55 weather stations.

Table 4: Mean differences between WIT3 and RTA precipitation projections for the 100 y return period rainfall events

		1 h storm		24 h storm	
GCM scenario	**Year**	**Mean (mm/h)**	**Standard deviation (mm/h)**	**Mean (mm/h)**	**Standard deviation (mm/h)**
CanESM RCP 8.5	2010	-2.84	1.70	-0.43	0.19
	2060	-1.72	1.69	-0.45	0.19
	2090	-0.96	1.96	-0.46	0.22
MPI-ESM LR RCP 8.5	2010	-2.48	1.73	-0.39	0.20
	2060	-1.37	1.72	-0.42	0.19
	2090	-0.73	1.96	-0.44	0.22

Incorporating projected temperature into the forecast resulted in an overall decrease in projected precipitation over the next 70 years, with the difference decreasing with time for the 1h storm. WIT3 design rainfall values for the 100 y, 1 h storm are, on average, 1.7 mm below those of RTA. The one exception is in Eastern Ontario, as Figure 9 shows, where 1 h storm intensities from the WIT3 model surpass those of the RTA model. While the risk in these areas appears minor, it does warrant further investigation. These differences could have significant

implications for climate change related risk and vulnerability assessments depending on the types of facilities and infrastructure.

The next chapter covers risk analysis based on future forecast of extreme precipitation and uncertainty analysis of future precipitation forecast based on ensemble methods. This analysis looks at variation in forecast of extreme precipitation values based on different GCM and RCP combination.

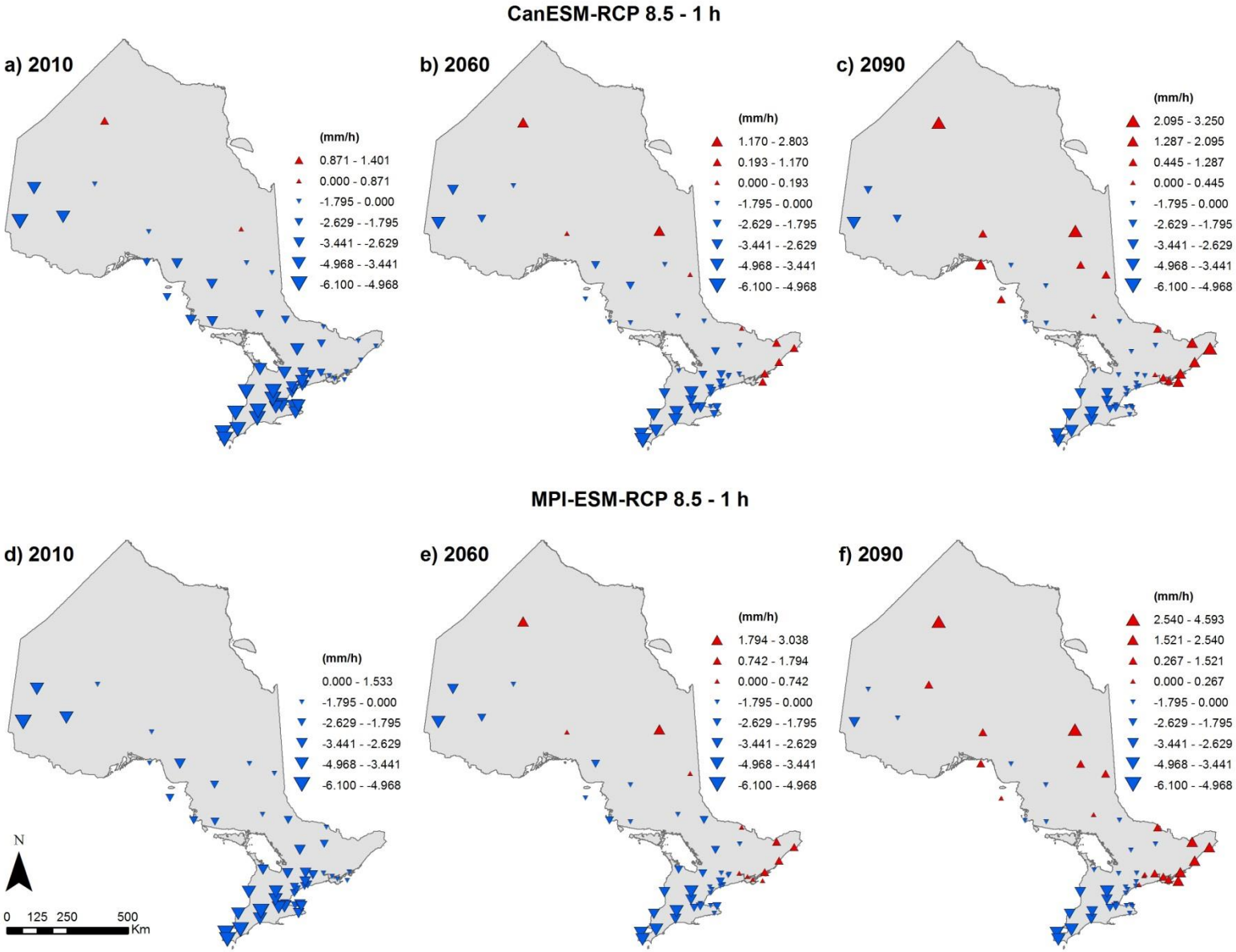

Figure 9: The difference between future 1 h extreme precipitation projections by WIT3 and RTA

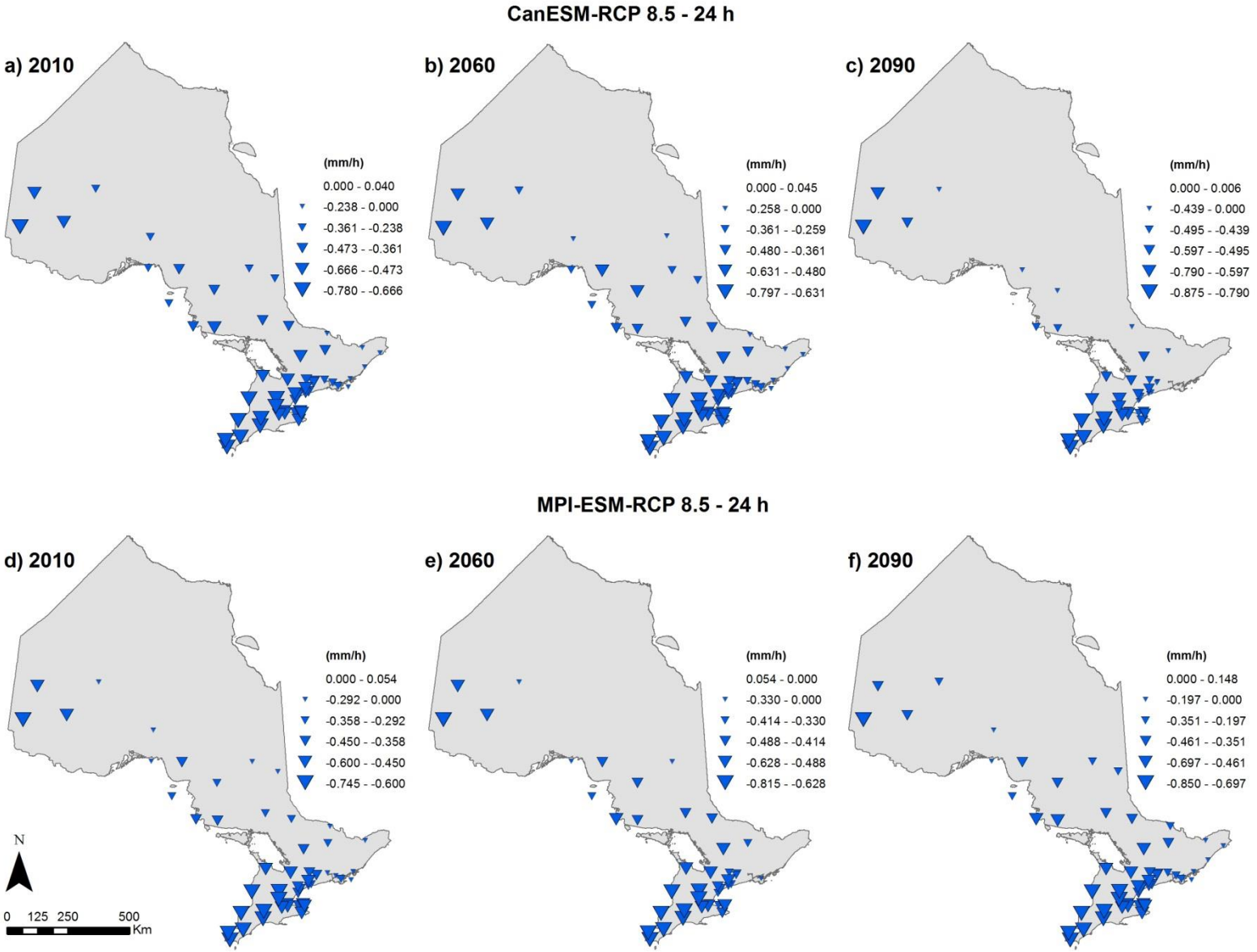

Figure 10: The difference between future 24 h extreme precipitation projections by WIT3 and RTA

Chapter 5: Risk and Uncertainty Analysis

5.1: Risk Analysis:

Figure 11shows a time series of expected annual maximum 24 h rainfall, the 100 y return period value, and the values produced by six different downscaled GCM and RCP combinations for St. Catharines Airport in Ontario. The red and black series have relatively small standard deviations because they represent precipitation quantiles. The green data series, with their much larger deviations, represents a GCM run. Chapter 1 shows how GCM precipitation predictions for historical runs are messy, with very low efficiency for precipitation predictions. Figure 11also demonstrates how precipitation intensity for the 24 h 100 y return period that WIT3 predicts successfully accommodates the peaks drawn by GCMs with various climate change scenarios.

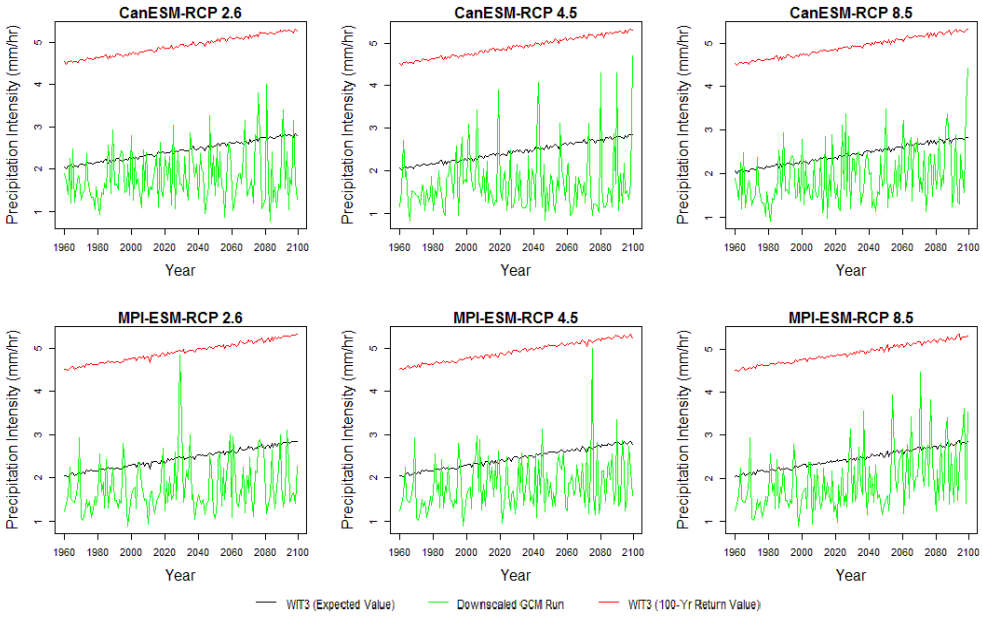

Figure 11: Time series of annual maximum 24 h rainfall, St. Catharines A, ON

Figure 11shows that time is the main driver of change in precipitation intensity in WIT3, while temperature contributes to mild fluctuations on top of the main linear trend. Figure 12 to

Figure 19 have similar fluctuations, which show the daily and hourly precipitation intensities that WIT3 predicts over the next century for various return periods and GCM-RCP combinations, at eight stations across Ontario. As Figure 12 to Figure 21, and Table 5 to Table 6 show, fluctuation in precipitation intensity prediction vary from 0.7 to 4.5%, which seems marginal as compared to percentage increase in precipitation intensities. Table 5 shows the percent increase in precipitation intensities by 2099 for eight stations across Ontario, with 2010 as base year, for various GCM-RCP combinations.

Table 5 and Table 6 show the percentage increase of precipitation intensities for eight sample stations from the 2010 base year to 2099. The 2 y return period ranges from 17% to a maximum of 34% for all GCMs and RCPs and for all durations. Similarly, the 100 y return period estimated increases in precipitation intensity ranges from 8% to 12% for all GCMs and RCPs and for all durations. Interestingly, the increase in future precipitation intensity for smaller storms (2 y) is greater than heavy storms (50 y, 100 y). This shows how smaller storms are expected to be more severe in future.

Table 5: Per cent increase in precipitation intensities by year 2099, with 2010 as base year

		CanESM 2.6 (%)	CanESM 4.5 (%)	CanESM 8.5 (%)	MPIESM 2.6 (%)	MPIESM 4.5 (%)	MPIESM 8.5 (%)	Maximum Precipitation Intensity (mm/h)	Minimum Precipitation Intensity (mm/h)	Fluctuation (%)
Armstrong	**1h 2y**	37.41	19.74	24.75	24.39	24.41	17.35	24.78	23.99	3.27
	1h 5y	27.35	14.86	18.54	18.22	18.34	14.88	31.36	30.57	2.57
	1h 10y	23.22	12.77	15.91	15.61	15.75	12.60	35.71	34.93	2.25
	1h 25y	19.50	10.84	13.48	13.21	13.37	11.32	41.22	40.43	1.94
	1h 50y	11.32	17.42	9.75	12.11	11.86	12.02	45.30	41.22	9.91
	1h 100y	10.28	15.76	8.87	11.00	10.77	10.92	49.35	48.57	1.62
Cornwall	**1h 2y**	20.82	26.66	25.85	22.12	25.58	23.50	24.73	24.22	2.13
	1h 5y	15.69	19.91	19.36	16.64	19.07	17.69	31.31	30.79	1.67
	1h 10y	13.49	17.06	16.60	14.30	16.32	15.20	35.67	35.15	1.47
	1h 25y	11.46	14.44	14.07	12.14	13.81	12.90	41.17	40.65	1.27
	1h 50y	10.31	12.96	12.63	10.91	12.39	11.60	45.25	44.74	1.15
	1h 100y	9.38	11.77	11.48	9.92	11.25	10.55	49.31	48.79	1.06
Cambridge	**1h 2y**	20.69	26.24	22.88	22.14	22.76	20.63	25.82	24.86	3.87
	1h 5y	15.77	19.85	17.40	16.88	17.17	15.78	32.40	31.44	3.06
	1h 10y	13.62	17.09	15.02	14.59	14.78	13.65	36.75	35.79	2.69
	1h 25y	11.62	14.54	12.81	12.45	12.56	11.67	42.26	41.84	1.00
	1h 50y	10.48	13.09	11.54	11.23	11.30	10.53	46.34	45.38	2.12
	1h 100y	9.55	11.91	10.52	10.23	10.28	9.60	50.39	49.43	1.95
Sudbury	**1h 2y**	20.71	28.58	22.14	21.33	25.09	18.73	24.76	24.41	1.43
	1h 5y	15.63	21.30	16.72	16.12	18.76	14.20	31.34	30.99	1.13
	1h 10y	13.45	18.23	14.38	13.87	16.08	12.24	35.69	35.34	0.99
	1h 25y	11.43	15.42	12.22	11.80	13.62	10.42	41.20	40.85	0.85
	1h 50y	10.29	13.83	11.00	10.62	12.23	9.39	45.28	44.93	0.78
	1h 100y	9.36	12.55	10.01	9.66	11.10	8.55	49.33	48.98	0.71

Table 6: Per cent increase in precipitation intensities by year 2099, with 2010 as base year

		CanESM 2.6 (%)	CanESM 4.5 (%)	CanESM 8.5 (%)	MPIESM 2.6 (%)	MPIESM 4.5 (%)	MPIESM 8.5 (%)	Maximum Precipitation Intensity (mm/h)	Minimum Precipitation Intensity (mm/h)	Fluctuation (%)
St. Catharines	**1h2Y**	20.86	25.35	23.40	23.10	22.84	21.29	25.77	24.93	3.37
	1h5Y	15.87	19.18	17.77	17.58	17.25	16.25	32.35	31.51	2.67
	1h10Y	13.70	16.51	15.33	15.17	14.84	14.05	36.71	35.87	2.34
	1h25Y	11.68	14.05	13.07	12.94	12.62	12.00	42.21	41.37	2.03
	1h50Y	10.53	12.65	11.78	11.66	11.35	10.82	46.29	45.45	1.85
	1h100Y	9.59	11.51	10.72	10.63	10.33	9.86	50.35	49.51	1.70
North Bay	**1h2Y**	22.59	28.54	23.32	20.68	24.96	18.65	24.99	24.48	2.09
	1h5Y	17.01	21.32	17.61	15.68	18.69	14.16	31.57	31.06	1.65
	1h10Y	14.63	18.26	15.15	13.52	16.02	12.21	35.93	35.41	1.45
	1h25Y	12.42	15.46	12.88	11.51	13.57	10.40	41.43	40.92	1.25
	1h50Y	11.17	13.88	11.59	10.37	12.19	9.37	45.51	45.00	1.14
	1h100Y	10.16	12.60	10.54	9.44	11.07	8.53	49.57	49.05	1.05
Kenora	**1h2Y**	22.64	29.96	21.15	24.17	21.40	17.33	25.97	24.85	4.52
	1h5Y	17.23	22.54	16.18	18.37	16.31	13.22	32.55	31.43	3.58
	1h10Y	14.88	19.36	14.01	15.86	14.09	11.43	36.91	35.78	3.14
	1h25Y	12.69	16.43	11.97	13.52	12.03	9.76	42.41	41.29	2.72
	1h50Y	11.44	14.78	10.81	12.18	10.85	8.80	46.49	45.37	2.48
	1h100Y	10.42	13.43	9.85	11.10	9.88	8.02	50.55	49.42	2.27
Hamilton	**1h2Y**	21.00	25.86	23.42	22.86	23.01	20.87	25.60	24.65	3.84
	1h5Y	15.94	19.53	17.76	17.37	17.32	15.91	32.18	31.23	3.03
	1h10Y	13.75	16.80	15.32	14.99	14.89	13.75	36.53	35.58	2.66
	1h25Y	11.72	14.29	13.04	12.78	12.64	11.73	42.04	41.09	2.30
	1h50Y	10.56	12.86	11.75	11.51	11.37	10.58	46.12	45.17	2.10
	1h100Y	9.61	11.70	10.70	10.49	10.33	9.64	50.17	49.22	1.92

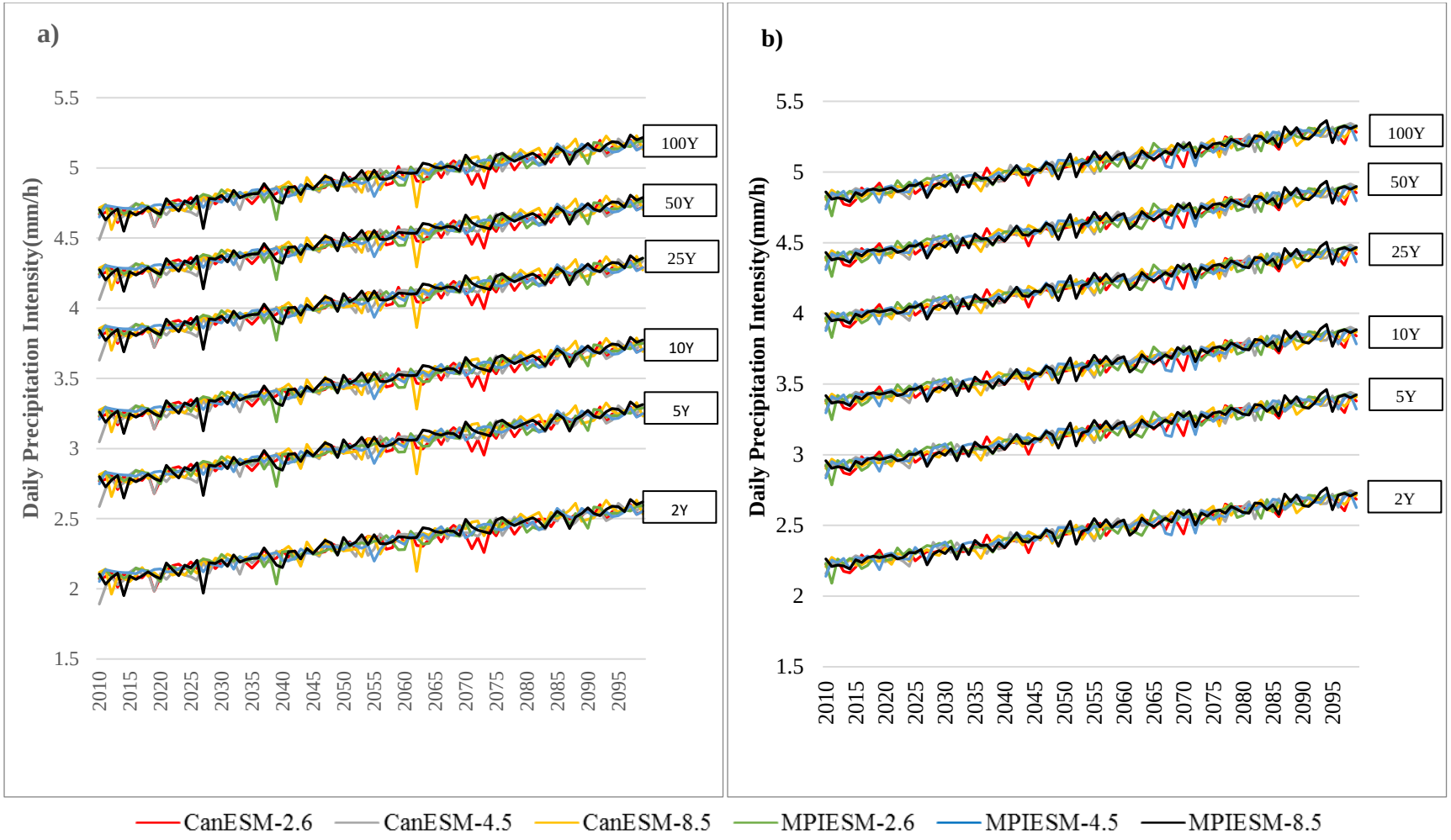

Figure 12: Daily precipitation intensity variation at a) Armstrong, b) Cambridge

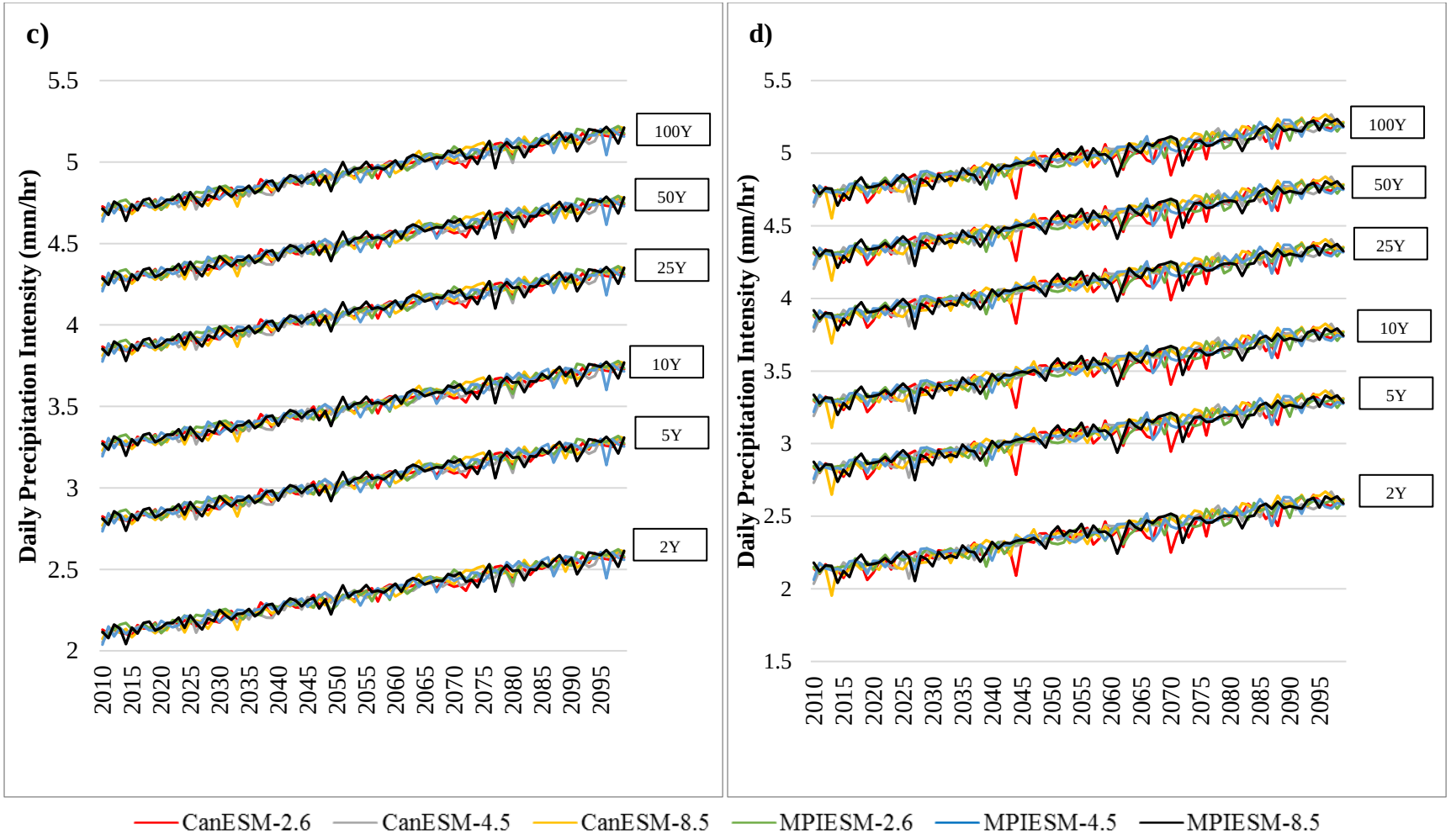

Figure 13: Daily precipitation intensity variation at c) Cornwall, d) Sudbury

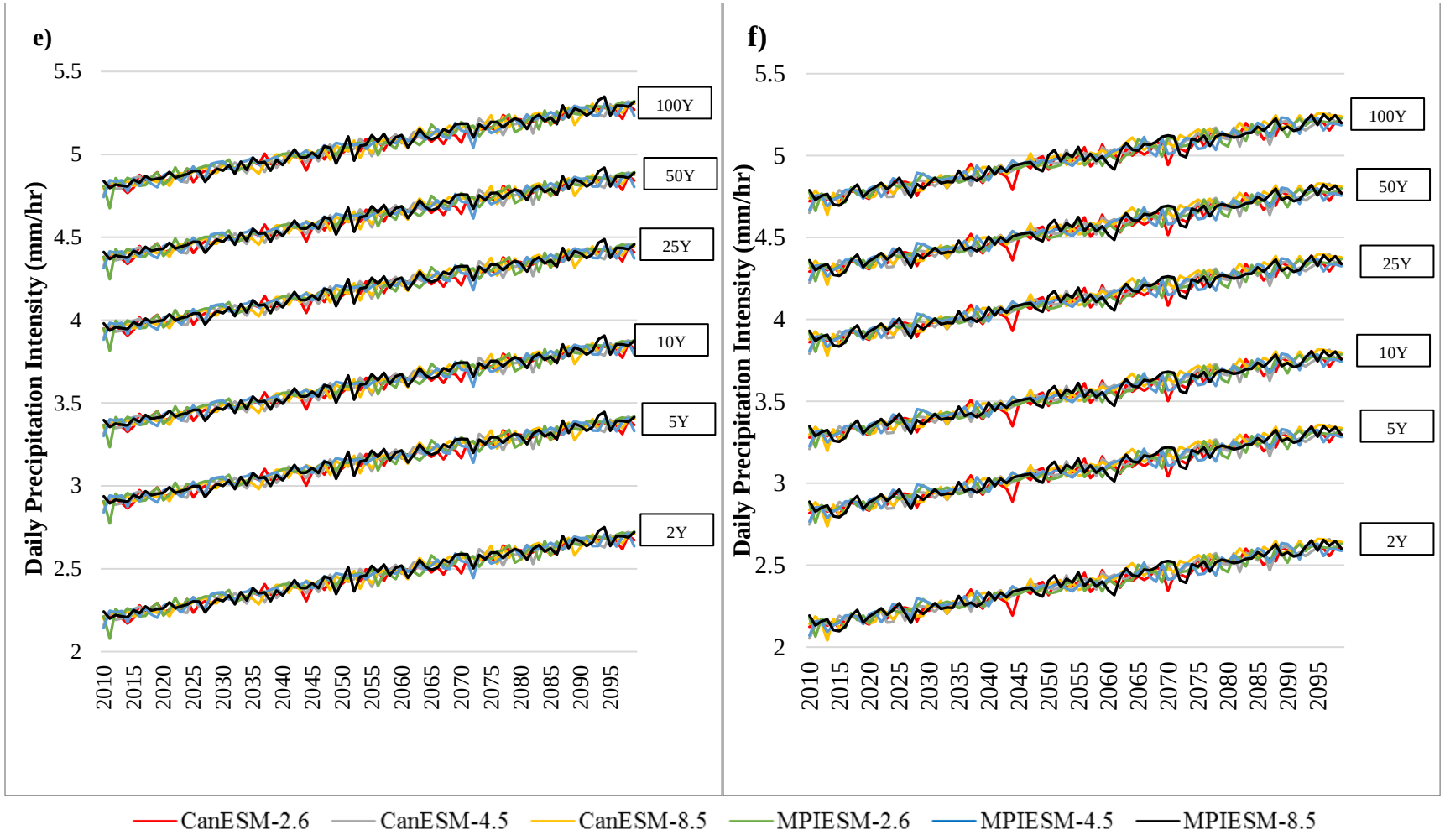

Figure 14: Daily precipitation intensity variation at e) St. Catharines, f) North Bay

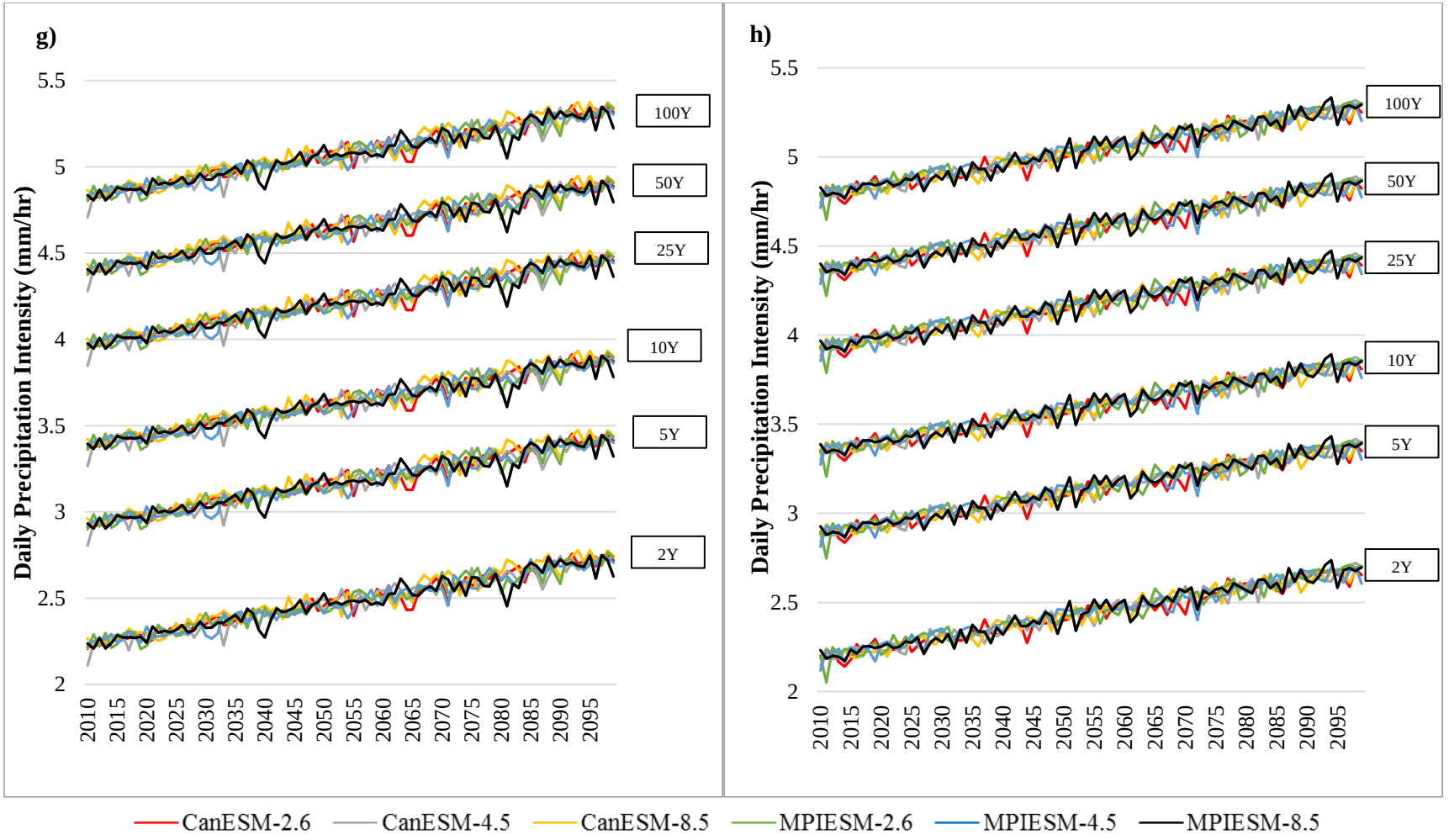

Figure 15: Daily precipitation intensity variation at g) Kenora h) Hamilton

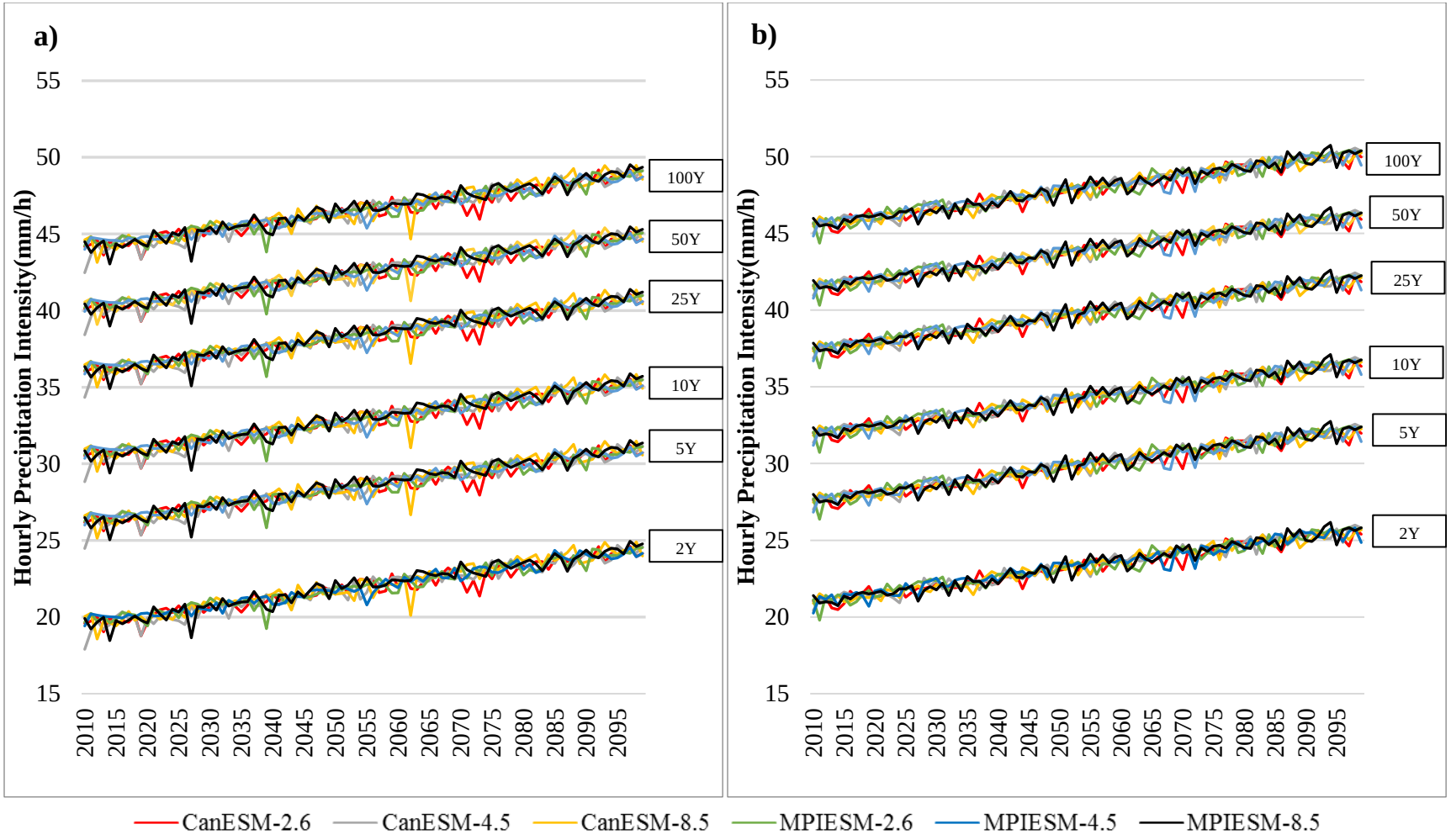

Figure 16: Hourly precipitation intensity variation at a) Armstrong, b) Cambridge

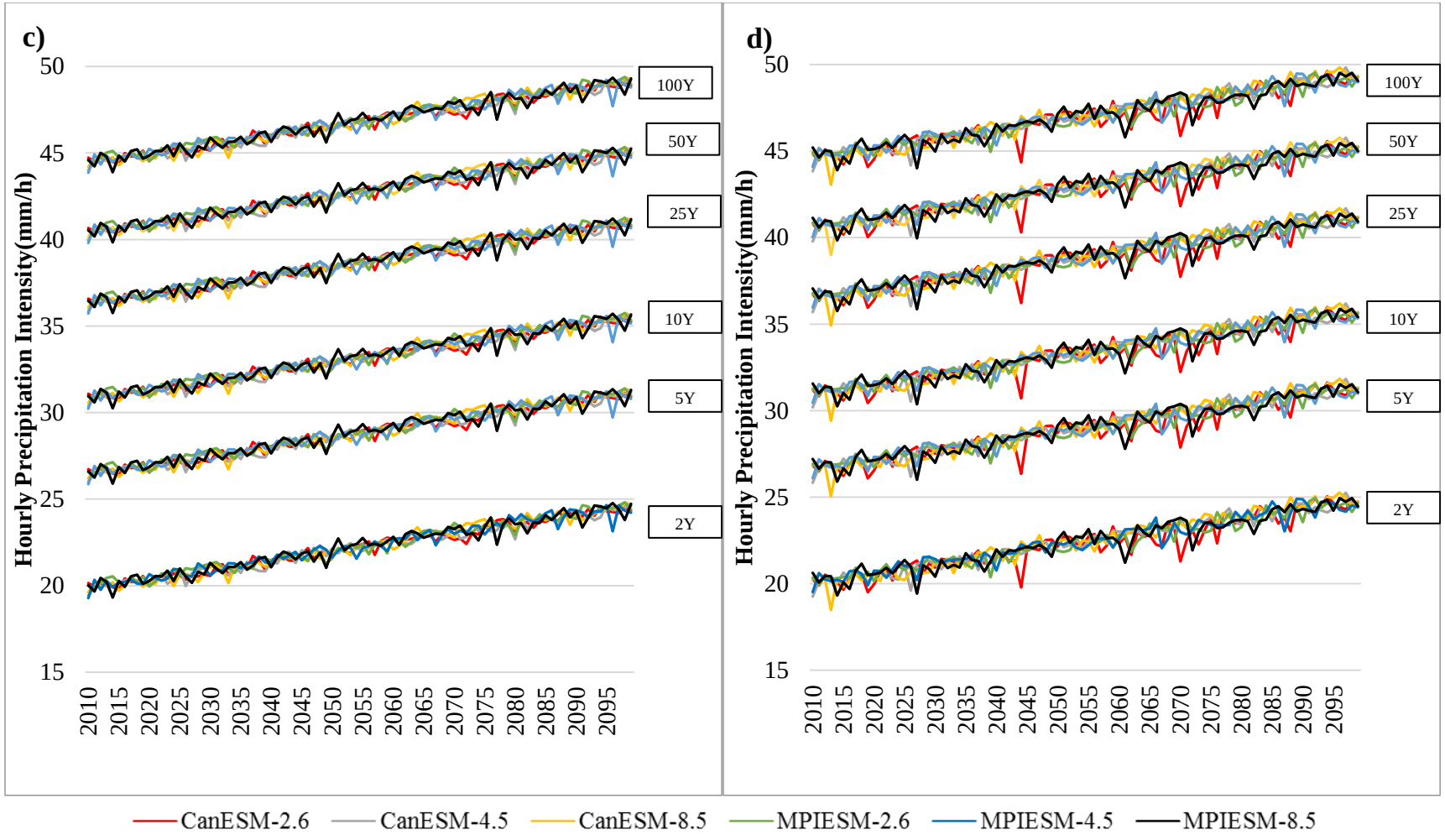

Figure 17: Hourly precipitation intensity variation at c) Cornwall, d) Sudbury

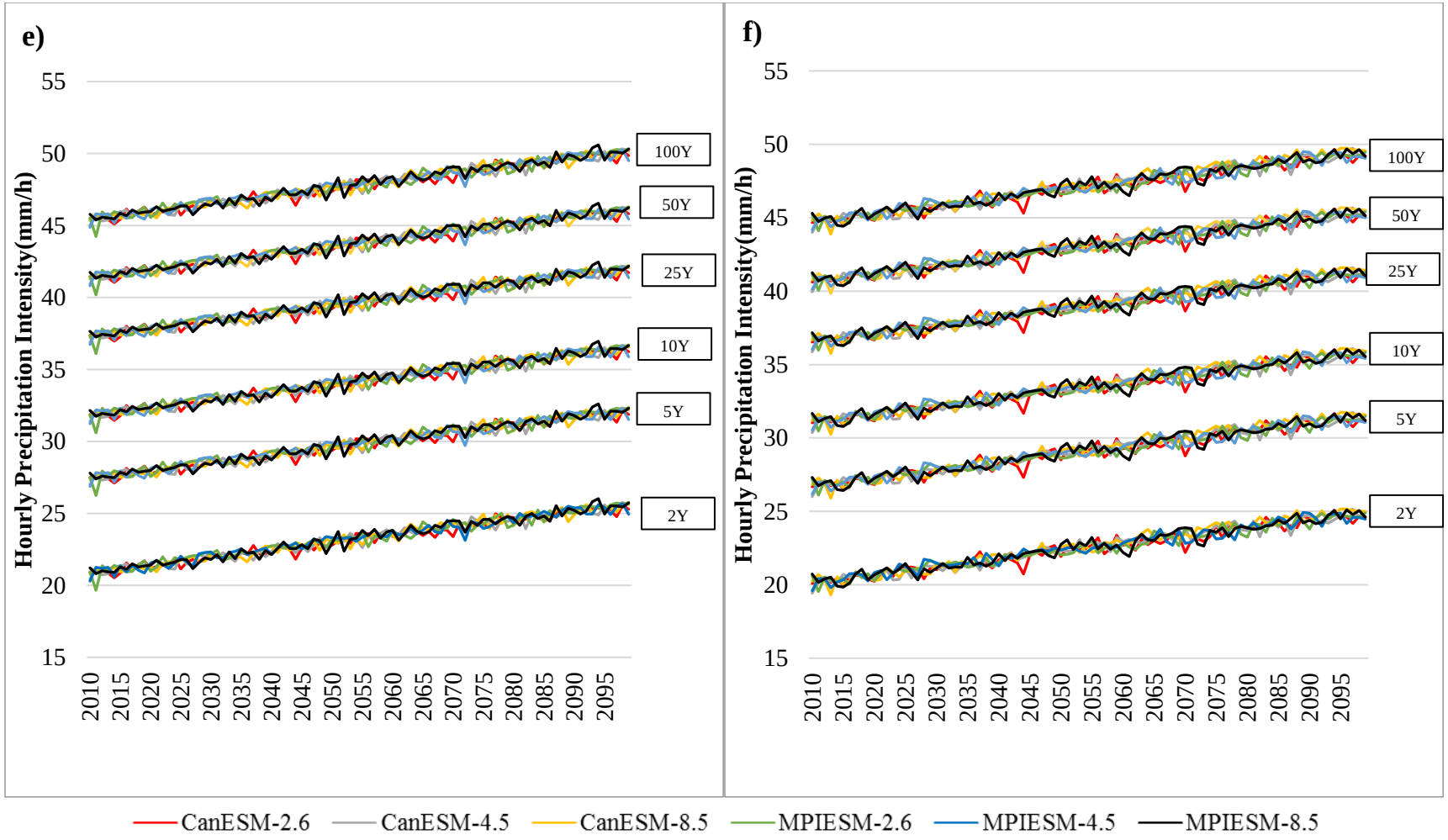

Figure 18: Hourly precipitation intensity variation at e) St. Catharines, f) North Bay

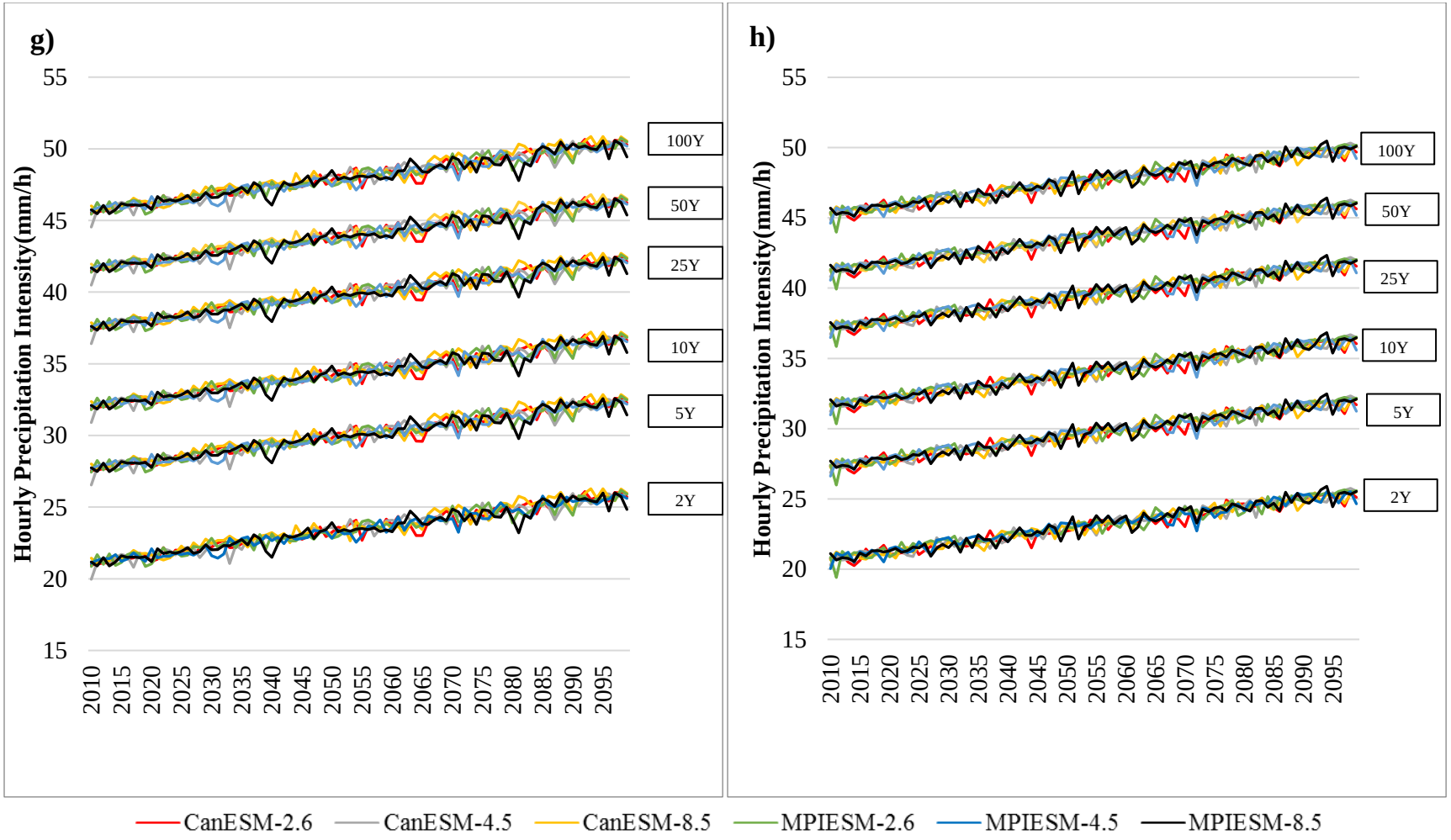

Figure 19: Hourly precipitation intensity variation at g) Kenora h) Hamilton

5.2: Sources of Uncertainty:

Predictions of the timing and magnitude of any future extreme event are associated with uncertainties in estimating future anthropogenic emissions of GHGs, land use changes, changes in the temperature, changes in the carbon cycle—especially the uptake of carbon in the oceans—and the challenges of understanding the relevant mechanisms, such as those from clouds and Ocean currents.

Different sources can help interpret the inherent uncertainties of climate models. 'Forcing uncertainty' uses future elements and aspects that are not a part of the climate system, but have the potential to affect it. One form of forcing uncertainty arises when one uses climate model simulations based on different scenarios for the concentrations of atmospheric GHGs, which depend entirely on the actions taken to control the GHG emissions (Cubasch *et al.*, 2001). In this study, they are incorporated as Representative Concentration Pathways (RCPs), as described in AR5. 'Initial condition uncertainty' involves uncertainty that arises from an initial state (Boundary conditions) or ensemble of states (Stainforth *et al.*, 2007) applied to the climate models.

Sciences, Hailegeorgis, & Burn (2009) mentioned that the main sources of uncertainties in assessing the impacts of climate change on extreme precipitation events can be from:

- GCMs; GHG scenarios;
- Downscaling techniques; and
- Impact assessment uncertainties:
- Model parameters: estimation of model parameters; and
- Data: data quality and sampling uncertainties.

Xu, Booij, & Tong, 2010, portrayed different sources of uncertainty in statistical modeling of extreme hydrological events. The results show that the uncertainty that originated from DSM is the largest, and could be 40% for a return period of 200 y. Similar results were found by (Mandal, Breach, & Simonovic, 2016). Using four GCMs, three RCPs, and six downscaling methods (DSMs). With the Campbell River basin in British Columbia as a case study, they showed that the selection of a downscaling method provides the largest amount of uncertainty when compared to the choice of GCM and emission scenario. The choice of GCM, however, provides a significant amount of uncertainty if downscaling methods are not considered.

The present study considers database from two global climate models, and three RCPs using one DSM, due to computational limitations. The study thus handles six different GCM-RCP ensemble outputs, for 111 stations across Ontario, and compares variability amongst them. From historical data, a temporal linear trend was identified, which forms the basis of this study, and it is assumed that the same linear trend is applicable in future (next century) as well, which may not be true for future. Thus, this is the limitation and source of uncertainty for the present study.

5.3: Uncertainty Analysis:

As Table 5 and Table 6 shows, the fluctuations in various GCM and RCP combinations vary from 2% to 4%. While this may seem small, consider that the maximum and minimum values of storm intensities for various return periods are large enough to overlap each other. This means that the minimum predicted value of rainfall intensity for the year 2075 may become the maximum possible rainfall intensity for the year 2050, due to variation in GCM and RCP selection.

Figure 20 and Figure 21shows non-exceedance probability of hourly precipitation intensities for eight stations across Ontario for the years 2010, 2025, 2050, 2075, and 2099. It also includes the maximum and minimum range of precipitation intensities predicted through six GCM-RCP ensembles. The maximum range of the 25 y storm overlaps the minimum precipitation intensity range of the 75 y storm. This indicates the non-stationarity in normal values, and the effect of climate change on extreme precipitation values.

Figure 12 to Figure 19 show reduction in recurrence interval, and increase (approximately double) in frequency of high intensity events, such as the 50 y and 100 y storms. The 100 y event will become the 50 y event, and the 50 y event will become the 25 y event after 2060. The doubling confirms that the intensity of extreme rainfall is increasing over the century, while the non-exceedance probability of a particular storm event is decreasing. For example, for St. Catharines, the probability that the precipitation intensity will not increase 30 mm/hr was 87-88% in 2010. In 2099, it will range from 67-70% depending on the GCM and RCP scenarios used.

Above results shows the necessity to build the climate resilient infrastructure, which again poses the need of best possible simulation of climate condition for future, which is dynamic in nature, and makes it almost mandatory to have design guidelines (here in this case IDF values) nonstationary. WIT3 serves this purpose by predicting nonstationary values of extreme precipitation intensities along with incorporation of three climate scenarios, which simulates best possible climate conditions for future years.

The next chapter summarizes the results, along with brief description about limitations of WIT3. It also covers future scope for extending this research.

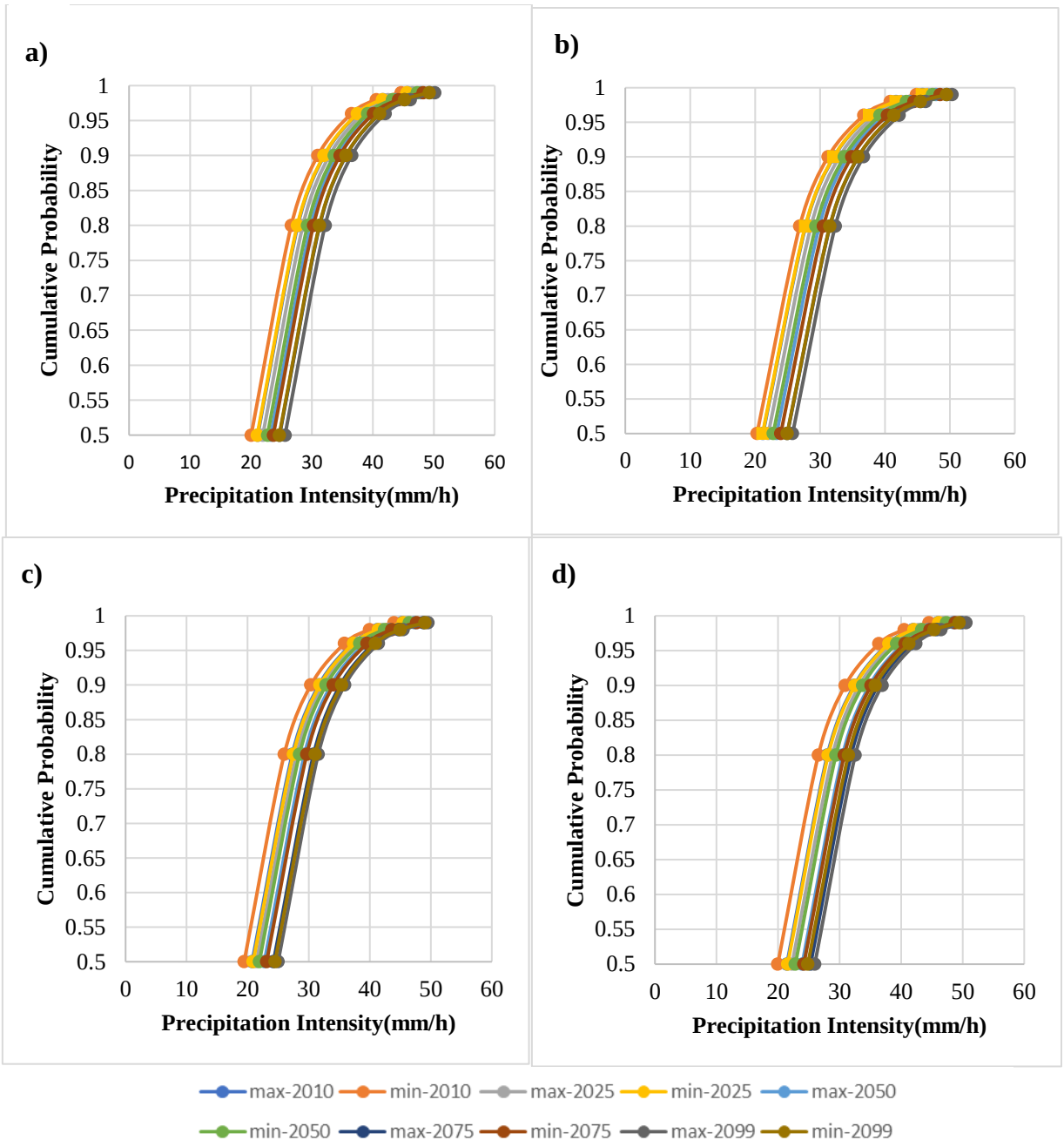

Figure 20: Non-exceedance probability of hourly precipitation intensities for four Ontario sites: a) Hamilton; b) St. Catharines; c) North Bay; and d) Kenora.

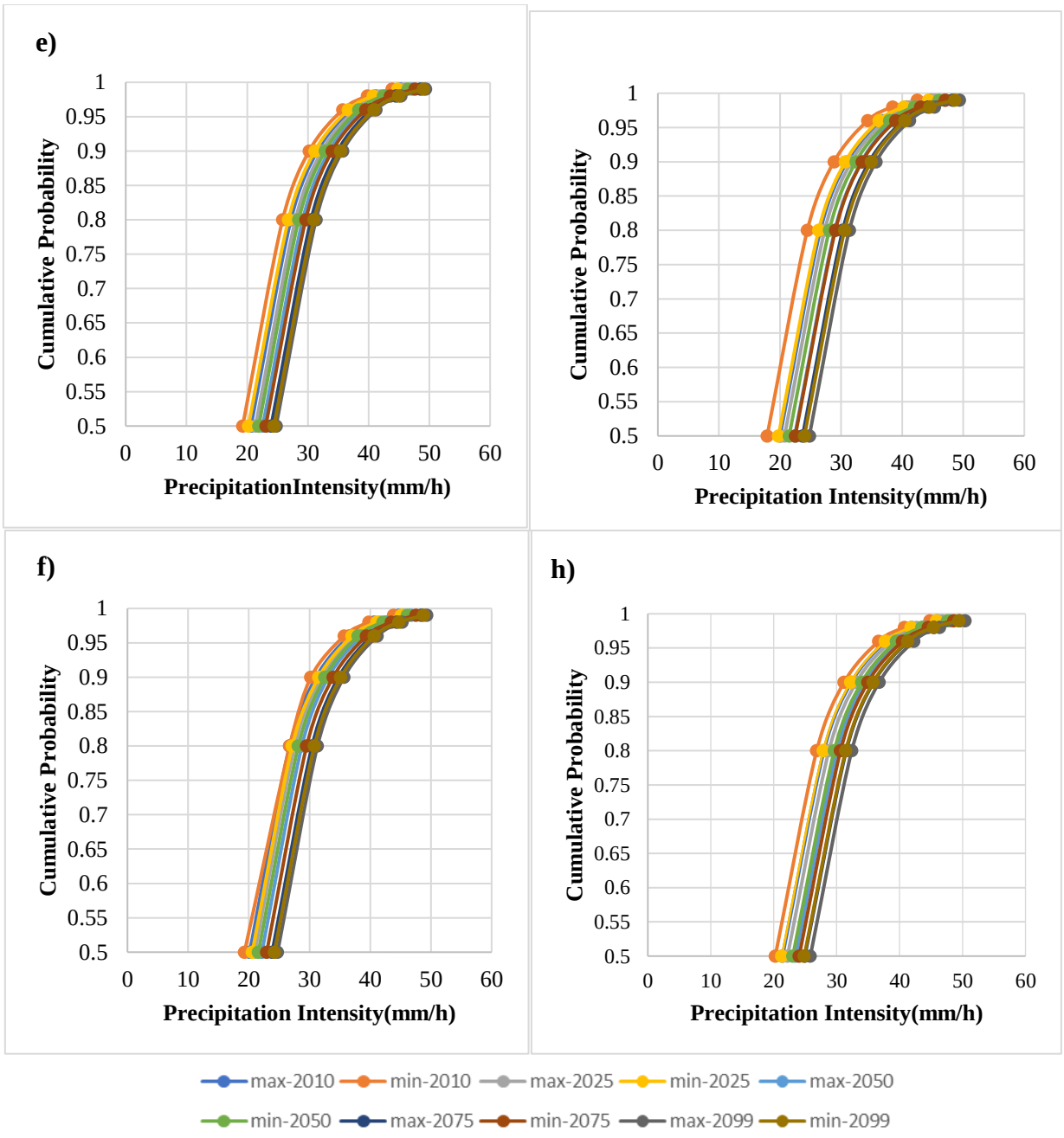

Figure 21: Non-exceedance probability of hourly precipitation intensities for four Ontario sites: e) Sudbury; f) Cornwall; g) Cambridge; and h) Armstrong.

Chapter 6: Summary and Future Scope of Study

6.1 Summary:

Global anthropogenic climate change has stimulated a variety of research focused on predicting future climate, and its effect on the earth. One of the most important aspects of these studies is to characterize possible changes in climate extremes (e.g., floods, droughts, high winds, etc.) The present study refines IDF curves for Ontario to provide new design guidelines MTO and MOECC.

Precipitation outputs are available for the future, from the CMIP5 database, that use different downscaling methods, and are available through PCIC and OCCDP. The resolutions of these outputs are 10 km and 25 km respectively. Although the database provided by PCIC is statistically downscaled and bias corrected, when precipitation intensity and its distribution was compared with actual precipitation data, for historical period 1960-2010, it did not match. Earlier studies (Soulis, Princz, & Wong, 2015) identified the regional temporal trend for extreme precipitation across Ontario. The only limitation of that study was absence of parameter, reflecting climate change. This study uses the same temporal trends, in association with local physiography, and temperature to forecast extreme rainfall. The new stochastic method of forecasting extreme precipitation, WIT3, has been developed to estimate the distribution of extreme rainfall events for Ontario locations. WIT3 is compared with existing RTA method, as well as the median IDF curve estimates from the OCCDP under the AR4:A1B scenario, and downscaled GCM data from PCIC. When comparisons were made during the historical period of 1960-2010, it was determined that WIT3 has the closest match of the empirical distribution of Ontario weather stations.

Forecasts of IDF curves were created until 2099, using temperature projections from two GCM models, namely CanESM and MPI-ESM, under three different RCP scenarios, RCP 2.6, RCP 4.5, and RCP 8.5.

Risk analyses of present studies use eight sites across Ontario, and future extreme rainfall predictions are made up to the year 2099. The study reveals that, percentage increases in rainfall intensities over the next century, are greater for short return periods, and lesser for heavy storm events. It also shows that the prediction of extreme rainfall intensities is sensitive to selection of GCM and RCP scenarios. The variation amongst the predictions is approximately 3 to 6 %, which seems small, but it is large enough to overlap the higher storm events. In many cases, the maximum hourly precipitation events for 50 y are overlapped with the 75y minimum hourly precipitation intensity curve after 2070 (see Figure 20 and Figure 21).

This study raises the need of a new normal, and the acceptance of non-stationarity in the context of varying climate. WIT3 will be incorporated into an online lookup tool, and should be tested for possible incorporation into the design standards of Ontario's infrastructure.

6.2: Limitations:

Although WIT3 represents the closest match with actual observations, there are times when it deviates. For short return periods, such as 2 y and 5 y, WIT3 slightly over-predicts results, while for higher return periods it sometimes under-predicts. WIT3 uses two GCMs, and one statistical downscaling method. This shows the potential for accommodating more GCMs and downscaling methods to reduce uncertainty, and more rigorous and accurate ensemble prediction, which was difficult in this study due to computational limitation. As this was a

regional study, the database was significantly large, which restricted the possibility of considering more GCMs and DSMs.

The present research assumes, linear temporal trend for future precipitation forecast, based on Soulis *et.al*(2016). It also considers that, precipitation distribution pattern would remain same, which means, standard error for the model remains same over the future years, and mean would increase, based on temporal trend and global warming.

6.3 Future Scope of Study:

The present study includes two GCMs and RCPs. More GCMs can reduce the uncertainty and improve the results. WIT3 is developed for Ontario. This study could be extended for the whole country to come up with best probable forecast for extreme rainfall over Canada, which can raise the country's resiliency to climate change by adapting to new nonstationary normal.

Chapter 7: References

Aldrian E. and Susanto R. Dwi, (2003) Identification of three dominant rainfall regions within Indonesia and their relationship to sea surface temperature, *International Journal of Climatology*, vol. 23, no. 12, pp. 1435–1452.

Alexander, L. V., Zhang, X., Peterson, T. C., Caesar, J., Gleason, B., Klein Tank, A. M. G., Vazquez-Aguirre, J. L. (2006). Global observed changes in daily climate extremes of temperature and precipitation. *Journal of Geophysical Research Atmospheres*, *111*(5). https://doi.org/10.1029/2005JD006290.

Allan RP, Soden BJ (2008) Atmospheric Warming and the Amplification of Precipitation Extremes. *Science* 321:1480–1484.

Allen, M. R., & Ingram, W. J. (2002). Constraints on future changes in climate and the hydrologic cycle. *Nature* **419**, 224-232 . doi:10.1038/nature01092.

Barnett DN, Brown SJ, Murphy JM, Sexton DMH, Webb MJ (2006) Quantifying Uncertainty in Changes in Extreme Event Frequency in Response to Doubled CO2 using a Large Ensemble of GCM Simulations. *ClimDyn* 26(5):489–511. doi:10.1007/S00382-005-0097-1.

Benyahya, L., Gachon, P., St-Hilaire, A., Laprise, R., (2014). Frequency analysis of seasonal extreme precipitation in southern Quebec (Canada): an evaluation of regional climate model simulation with respect to two gridded datasets. *Hydrol.Res*. 45 (1), 115–133. http://dx.doi.org/10.2166/nh.2013.066.

Berg, P., Haerter, J. O., Thejll, P., Piani, C., Hagemann, S., & Christensen, J. H. (2009). Seasonal characteristics of the relationship between daily precipitation intensity and surface temperature. *Journal of Geophysical Research Atmospheres*, 114(18), 1–9. https://doi.org/10.1029/2009JD012008.

Black E.(2005), The relationship between Indian Ocean sea-surface temperature and East African rainfall, *Philosophical Transactions of the Royal Society A*, 363(1826), pp. 43–47.

Charles, O., Patrick, W., 2015. Uncertainty in calibrating generalised Pareto distribution to rainfall extremes in Lake Victoria basin. *Hydrology Research* 46(3):356–376 .

Cooley D. (2013) Return Periods and Return Levels Under Climate Change. In: AghaKouchak A., Easterling D., Hsu K., Schubert S., Sorooshian S. (eds) Extremes in a Changing Climate. Water Science and Technology Library, vol 65. Springer, Dordrecht.

Cubasch, U., G.A. Meehl, G.J. Boer, R.J. Stouffer, M. Dix, A. Noda, C.A. Senior, S. Raper and K.S. Yap, Projections of future climate change, in Climate Change 2001: The Scientific Basis: Contribution of WGI to the Third Assessment Report of the IPCC, edited by J.T. Houghton et al., pp. 525-582, Cambridge University Press, New York, 2001.

Douglas, E. M., Vogel, R. M., and Kroll, C. N. (2000). Trends in floods and low flows in the United States: Impact of spatial correlation. *J. Hydrol.*, 240(1–2), 90–105.

El Adlouni, S., Ouarda, T.B.M.J., Zhang, X., Roy, R. and Bobée, B. (2007) Generalized maximum likelihood estimators for the nonstationary generalized extreme value model. *Water Resources Research*, 43.

Emori, S., and Brown, S. J. (2005). Dynamic and thermodynamic changes in mean and extreme precipitation under changed climate. *Geophysical Research Letters*, 32(17).

Enfield, D. B., Mestas-Nunez, A. M., and Trimble, P. J. (2001). The Atlantic Multidecadal Oscillation and its relation to rainfall and river flows in the continental U.S. *Geophys. Res. Lett.*, 28(10), 2077–2080.

Franks, S. W., and Kuczera, G. (2002). Flood frequency analysis: Evidence and implications of secular climate variability, New South Wales. *Water Resour. Res*., 38(5), 20-1–20-7.

Gilroy, K. L., and McCuen, R. H. (2012). A nonstationary flood frequency analysis method to adjust for future climate change and urbanization. *J. Hydrol*., 414–415(1), 40–48.

Giorgi, F. and R. Francisco, (2000). Evaluating Uncertainties in the Prediction of Regional Climate Change. *Geophysical Research Letters*, **27** (9): 1295-1298.

Griffis, V., and Stedinger, J. R. (2007). Incorporating climate change and variability into bulletin 17B LP3 model. Proc., World Environmental and Water Resources Congress, ASCE, Reston, VA, 1–8.

Groisman, Pavel Ya, et al. (2005) Trends in intense precipitation in the climate record. *Journalof climate*, 18.9 .

Gudmundsson, L., J. B. Bremnes, J. E. Haugen, and T. Engen-Skaugen,(2012). Technical Note: Downscaling RCM precipitation to the station scale using statistical transformations - a comparison of methods. *Hydrology and Earth System Sciences*, **16**: 3383–3390, doi:10.5194/hess-16-3383-2012.

Hassanzadeh E, Nazemi A, Elshorbagy, A. (2013) Quantile-Based Downscaling of Precipitation using Genetic Programming: Application to IDF Curves in the City of Saskatoon. *J. Hydrol. Eng.*, 10.1061/(ASCE)HE.1943-5584.0000854.

Hejazi, M. I., and Markus, M. (2009). Impacts of urbanization and climate variability on floods in northeastern Illinois. *J. Hydrol. Eng*., 10.1061/(ASCE)HE.1943-5584.0000020, 606–616.

Hogg W.D., Carr D.A., Routledge B.(1989). *Rainfall Intensity–Duration–Frequency Values for Canadian Locations*. Environment Canada, Atmospheric Environment Service: Ottawa.

IPCC (2013) Summary for Policymakers. In: *Climate Change* 2013: *The Physical Science Basis*, Contribution of Working Group I to the Fifth Assessment Report of the Intergovernmental Panel on Climate Change, Cambridge University Press, Cambridge, United Kingdom and New York, NY, USA. https://www.ipcc.ch/pdf/assessment-report/ar5/wg1/WGIAR5_SPM_brochure_en.pdf.

J. Shukla and B. M. Misra,(1977) Relationships between sea surface temperature and wind speed over the central Arabian Sea, and monsoon rainfall over India, *Monthly Weather Review*, 105, pp. 998–1002, 1977.

Jain, S., and Lall, U. (2000). Magnitude and timing of annual maximum floods: Trends and large-scale climatic associations for the Blacksmith Fork River, Utah. *Water Resour. Res.*, 36(12), 3641–3651.

Jain, S., and Lall, U. (2001). Floods in a changing climate: Does the past represent the future? *Water Resour. Res.*, 37(12), 3193–3205.

Kao SC, Ganguly AR (2011) Intensity, Duration, and Frequency of Precipitation Extremes Under 21st-Century Warming Scenarios. *J Geophys Res* 116(D16), D16119. doi:10.1029/2010JD015529.

Katz, R., et al., (2002),Statistics of extremes in hydrology. *Advances in Water Resources*, 25,12871304.

Katz, R.W. (2013),Statistical methods for nonstationary extremes *Extremes in a Changing Climate*, Springer Netherlands.

Kiem, A. S., Franks, S. W., and Kuczera, G. (2003). Multi-decadal variability of flood risk. *Geophys. Res. Lett.*, 30(2), GL015992.

Knutson, T. R., et al. (2010). Tropical cyclones and climate change. *Nat. Geosci.*, 3(3), 157–163.

Konrad, C. P., and Booth, D. B. (2002). "Hydrologic trends associated with urban development for selected streams in the Puget Sound Basin, western Washington." USGS Water Resources Investigations Rep. 02-4040, United States Geological Survey, Tacoma, WA.

Lins, H. F., and Slack, J. R. (1999). Streamflow trends in the United States. *Geophys. Res. Lett.*, 26(2), 227–230.

Mailhot A, Duchesne S, Caya D, Talbot G (2007) Assessment of Future Change in Intensity-Duration-Frequency(IDF) Curves for Southern Quebec Using the Canadian Regional Climate Model (CRCM). *J Hydrol* 347:197–210.

Mandal, S., Breach, P.A. and Simonovic, S.P. (2016) Uncertainty in Precipitation Projection under Changing Climate Conditions: A Regional Case Study. *American Journal of Climate Change*, 5, 116-132. http://dx.doi.org/10.4236/ajcc.2016.51012.

Mantua, N. J., Hare, S. R., Zhang, Y., Wallace, J. M., and Francis, R. C. (1997). "A Pacific Interdecadal Climate Oscillation with impacts on salmon production." Bull. Am. Meteorol. Soc., 78(6), 1069–1079.

Maurer, E., H. Hidalgo, T. Das, M. Dettinger, and D. Cayan, (2010). The utility of daily large-scale climate data in the assessment of climate change impacts on daily streamflow in California. *Hydrology and Earth System Sciences*, **14**(6): 1125–1138, doi:10.5194/hess-14-1125-2010.

McCabe, G. J., and Wolock, D. M. (2002). "A step increase in streamflow in the conterminous United States." *Geophys. Res. Lett*., 29(24), GL015999.

Meehl G A, Arblaster J M and Tebaldi C (2005) Understanding future patterns of increased precipitation intensity in climate model simulations *Geophys. Res. Lett.* 32 L18719.

Menendez, M., and Woodworth, P. L. (2010). Changes in extreme high water levels based on a quasi-global tide-gauge data set. *J. Geophys.Res. Oceans*, 115(C10), JC005997.

Milly, P. C. D., et al. (2008). "Stationarity is dead: Whither water management?" *Science*, 319(5863), 573–574.

Min, S.-K., Zhang, X., Zwiers, F. W., & Hegerl, G. C. (2011). Human contribution to more-intense precipitation extremes. *Nature*, *470*(7334), 378–381. https://doi.org/10.1038/nature09763.

Mirhosseini G, Srivastava P, Stefanova L (2013) The Impact of Climate Change on Rainfall Intensity–Duration–Frequency (IDF) Curves in Alabama. *Reg Environ Change* 13(S1):25–33. doi:10.1007/s10113-012-0375-5.

Moise F., Colman R.A., and Brown J.R. (2012) Behind uncertainties in projections of Australian tropical climate: analysis of 19 CMIP3 models, *Journal of Geophysical Research*, vol.117, Article ID D10103.

Nguyen VTV, Nguyen TD, Cung A (2007), A Statistical Approach to Downscaling of Sub-Daily Extreme Rainfall Processes for Climate-Related Impact Studies in Urban Areas. *Water Science & Technology: Water Supply* 7(2):183. doi:10.2166/ws.2007.053.

Olsen, J. R., Stedinger, J. R., Matalas, N. C., and Stakhiv, E. Z. (1999). "Climate variability and flood frequency estimation for the Upper Mississippi and Lower Missouri rivers. *J. Am. Water Resour. Assoc*.,35(6), 1509–1523.

Pacific Climate Impacts Consortium (2017). Statistically downscaled climate scenarios", https://pacificclimate.org/data/statistically-downscaled-climate-scenarios.

Park, J., Obeysekera, J., Barnes, J., Irizarry, M., and Park-Said, W. (2010). Climate links and variability of extreme sea level events at Key West,Pensacola, and Mayport Florida. *J. Waterway*, Port, Coastal, Ocean Eng., 10.1061/(ASCE)WW.1943-5460.0000052, 350–356.

Park, J., Obeysekera, J., Irizarry, M., Barnes, J., Trimble, P., and Park-Said, W. (2011). Storm surge projections and implications for water management in south Florida, *Clim. Change*, 107(1–2),109–128.

Peck A, Prodanovic P, Simonovic SP (2012) Rainfall Intensity Duration Frequency Curves Under ClimateChange: City of London, Ontario, Canada. *Canadian Water Resources Journal* 37(3):177–189. doi:10.4296/cwrj2011-935.

Peixoto J P and Oort A H (1992) *Physics of Climate* (New York: AIP)

Pielke, R. A., Sr., et al. (2007). An overview of regional land-use and land-cover impacts on rainfall.Tellus B, 59(3), 587–601.

Prodanovic, P. and Simonovic, S.P. (2007). Impacts of Changing Climatic Conditions in Upper Thames River basin. *Canadian Water Resources,* 32(4):265-284.

Rajeevan M.,Pai,D.S. and Thapliyal V.,(1998) Spatial and temporal relationships between global land surface air temperature anomalies and Indian summer monsoon rainfall, *Meteorology Land Atmospheric Physics*, vol. 66, no. 3-4, pp. 157–171.

Sarhadi, A. and E.D. Soulis, (2017). Time-varying extreme rainfall intensity-duration-frequency curves in a changing climate. *Geophysical Research Letters*, 44. doi:10.1002/2016GL072201.

Sciences, A., Hailegeorgis, T. T., & Burn, D. H. (2009). Uncertainty Assessment of the Impacts of Climate Change on Extreme Precipitation Events. *Risk Management*, (December).

Seglenieks, F. (2009). *Creation of a Gridded Time Series of Hydrological Variables for Canada*. Waterloo, Ontario: University of Waterloo. PhD Thesis.

Solaiman TA, King LM, Simonovic SP (2011) Extreme Precipitation Vulnerability in the Upper Thames River basin: Uncertainty in Climate Model Projections. *Int J Climatol* 31:2350–2364. doi:10.1002/joc.2244.

Solaiman TA, Simonovic SP (2010) National Centers for Environmental Prediction-National Center forAtmospheric Research (NCEP-NCAR) Reanalyses Data for Hydrologic Modelling on a Basin ScaleCan J Civ Eng 37(4):611–623.

Solaiman TA, Simonovic SP (2011) Development of Probability Based Intensity-Duration-Frequency Curves under Climate Change. Water Resources Research Report no. 072, Facility for Intelligent Decision Support,Department of Civil and Environmental Engineering, London, Ontario, Canada, 89 pages. ISBN: (print)978–0–7714–2893–7; (online) 978–0–7714–2900–2.

Soulis, E.D., A. Sarhadi, M. Tinel, M. Suthar, 2016. Extreme precipitation time trends in Ontario, 1960–2010. *Hydrological Processes*. **30** (22): 4090-4100, doi: 10.1002/hyp.10969.

Srivastav, R. K., Schardong, A., & Simonovic, S. P. (2014). Equidistance Quantile Matching Method for Updating IDFCurves under Climate Change. *Water Resources Management*, *28*(9), 2539–2562. https://doi.org/10.1007/s11269-014-0626-y.

Stainforth, D. A., M. R. Allen, E. R. Tredger, and L. Smith (2007), Confidence and uncertainty and decision-support relevance in climate predictions, Philos. Trans. R. Soc., Ser. A, 365, 2145–2161.

Stephens G L (1990) On the relationship between water vapor over the oceans and sea surface temperature *J. Clim.* 3 634–45.

Strupczewski, W. G., Singh, V. P., and Mitosek, H. T. (2001). Nonstationary approach to at-site flood frequency modeling. III. Flood frequency analysis of Polish rivers. *J. Hydrol.*, 248(1), 152–167.

Sun Y, Solomon S, Dai A and Portmann R W (2006) How often does it rain? *J. Clim.* (19) 916–34.

Sveinsson, O.G.B., J.D. Salas, and D.C. Boes, (2005),Prediction of extreme events in hydrologic processes that exhibit abrupt shifting patterns, *Journal of Hydrologic Engineering*, 10(4), 315-326.

Tanarhte M, Hadjinicolaou P, Lelieveld J. (2012). Intercomparison of temperature and precipitation data sets based on observations in the Mediterranean and the Middle East. *Journal of Geophysical Research* **117**: D12102. DOI: 10.1029/2011JD017293.

Trenberth K E, Dai A, Rasmussen R M and Parsons D B 2003 The changing character of precipitation *Bull. Am. Meteorol. Soc.* 84 1205–17.

Villarini, G., Smith, J. A., Serinaldi, F., Bales, J., Bates, P. D., and Krajewski, W. F. (2009b). Flood frequency analysis for nonstationary annual peak records in an urban drainage basin. *Adv. Water Resour.*,32(8), 1255–1266.

Vogel, R. M., Yaindl, C., and Walter, M. (2011). "Nonstationarity: Floodmagnification and recurrence reduction factors in the United States." *J. Am. Water Resour. Assoc*., 47(3), 464–474.

Wentz, F. J. and Schabel, M. (2000) Precise climate monitoring using complementary satellite data sets. *Nature*, **403,** 414–416.

Westra, S., Fowler, H. J., Evans, J. P., Alexander, L. V., Berg, P., Johnson, F., Roberts, N. M. (2014). Future changes to the intensity and frequency of short-duration extreme rainfall. *Reviews of Geophysics*. Blackwell Publishing Ltd. https://doi.org/10.1002/2014RG000464.

Wilcox EM, Donner LJ (2007) The Frequency of Extreme Rain Events in Satellite Rain-Rate Estimates and Atmospheric General Circulation Model. *J Clim* 20(1):53-69.

Xu, Y. P., Booij, M. J., & Tong, Y. B. (2010). Uncertainty analysis in statistical modeling of extreme hydrological events. *Stochastic Environmental Research and Risk Assessment*, *24*(5), 567–578. https://doi.org/10.1007/s00477-009-0337-8.

Zhu, J., Forsee, W., Schumer, R., & Gautam, M. (2013). Future projections and uncertainty assessment of extreme rainfall intensity in the United States from an ensemble of climate models. *Climatic Change*, *118*(2), 469–485. https://doi.org/10.1007/s10584-012-0639-6.

Appendix-A: Application of IDF and Extreme Rainfall Values

The IDF curves act as a design tool for most urban and rural infrastructure. High flood levels define the plinth levels of all structures. These high flood levels, shown in Figure A-1, are drawn based on the maximum expected runoff in that area. Different structures are built with varying lengths of design life. Highways and bridges are built with a minimum life span of 75 to 100 years, whereas sewer lines are designed for minimum 10 to 25 years, depending on its scale and importance. Rainfall-runoff models consider total rainfall intensity as an input, develop a hyetograph based on a design storm and its recurrence interval, prepares a hydrograph based on rainfall and site conditions, and gives runoff as an output. This helps compute storm water runoff and its management, which is a major concern for almost all the cities across Canada.

Figure A-1: High Flood Levels

When rain falls on an urban area, some rainwater falls on impervious surfaces, which wets the surface, fills depression areas, partly evaporates, and finally turns into surface runoff. The rainwater that falls on pervious surface with vegetation is stored in stems and leaves, or in the absence of vegetation contributes to groundwater. Water that infiltrates soil may move

laterally through the upper soil horizons towards the stream as interflow. Water that percolates the lower soil horizons becomes ground water.

The transport of surface runoff in urban catchments starts with overland flow and quickly joins the storm water drain network. The formation of runoff may be graphically presented by plotting hydrographs. Such hydrographs represent integrated effects of rainfall and catchment characteristics, such as the area, shape surface cover, depression and infiltration capacities, land use, drainage patterns, surface and drainage slopes, sewer, channel, and stream characteristics. The magnitudes of peak discharges, and the shapes of these hydrographs, are of interest for the layout of urban drainage systems. Figure A-2 summarizes the principles of storm water runoff development, and its possible superimposition with dry weather flow.

In this research, nonstationary IDF values, and extreme rainfall intensities are predicted across Ontario. For each station, we can develop hyetograph and hydrograph, based on WIT3 output, which are valuable and basic inputs for rainfall-runoff models. These models are used for flood prediction and the drawing of flood lines. This is one of the major inputs in infrastructure design such as highways, bridges, and dams. Storm water runoff computation is also useful for designing capacity of waste water treatment plants in areas with combined sewer systems.

It is very important to have extreme rainfall forecast to be sensitive and accurate enough to be able to adapt with varying climate conditions. WIT3 has not only forecasted nonstationary extreme precipitation intensities, but also tied it up with future land use change, socio-economic conditions (using RCP) along with local topography and temperature change over the next century.

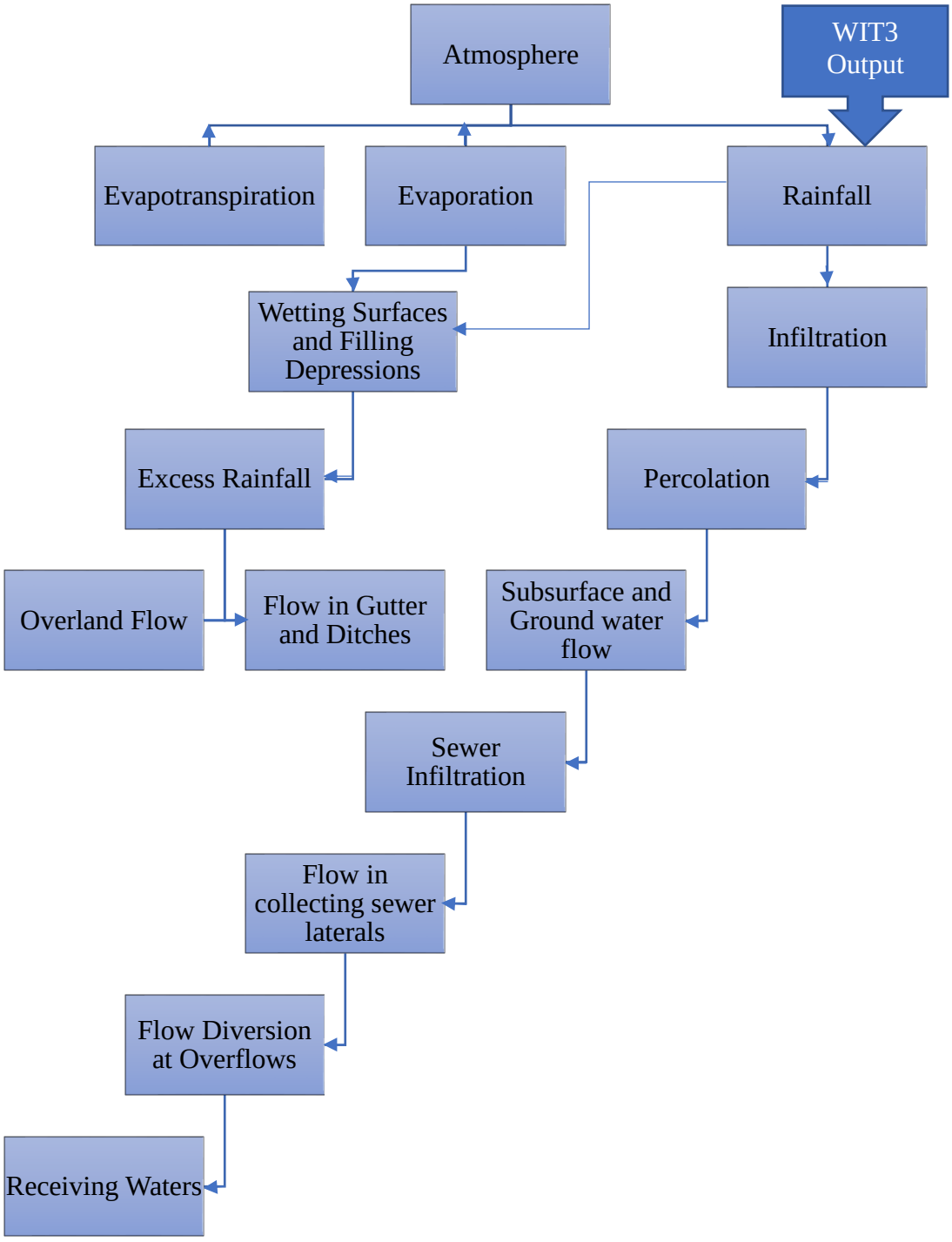

Figure A-2: Development of storm water runoff and flow in storm water sewer systems (source: Manual on drainage in urbanized areas,Vol:1)

Appendix-B: IDF Curve Projections for St. Catharines A, Ontario

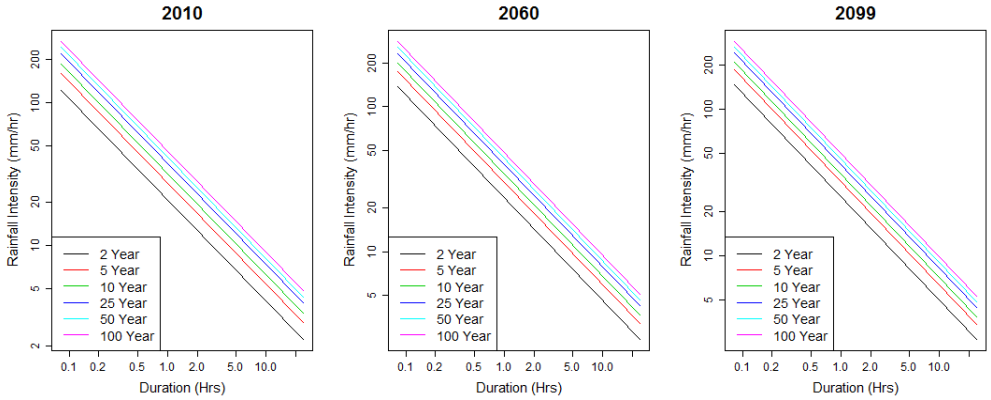

(a) CanESM RCP 2.6

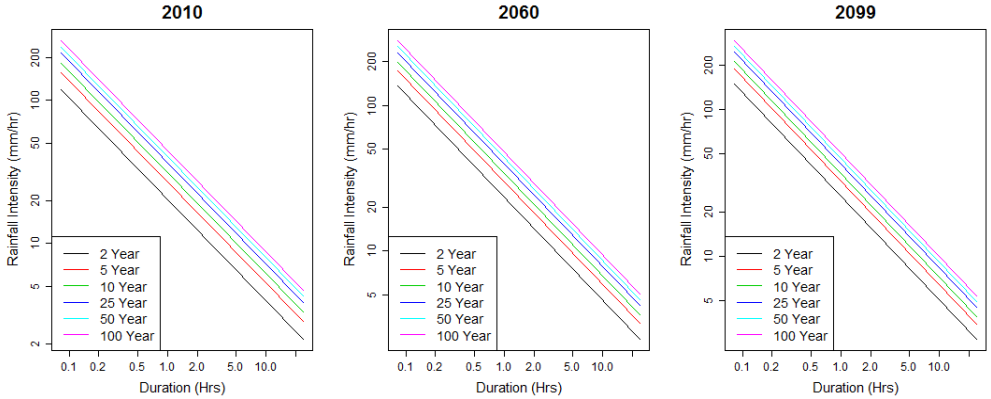

(b) CanESM RCP 4.5

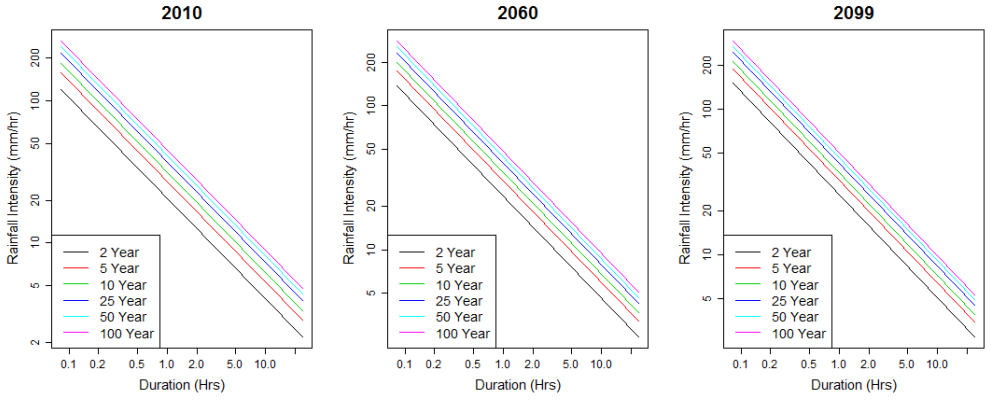

(c) CanESM RCP 8.5

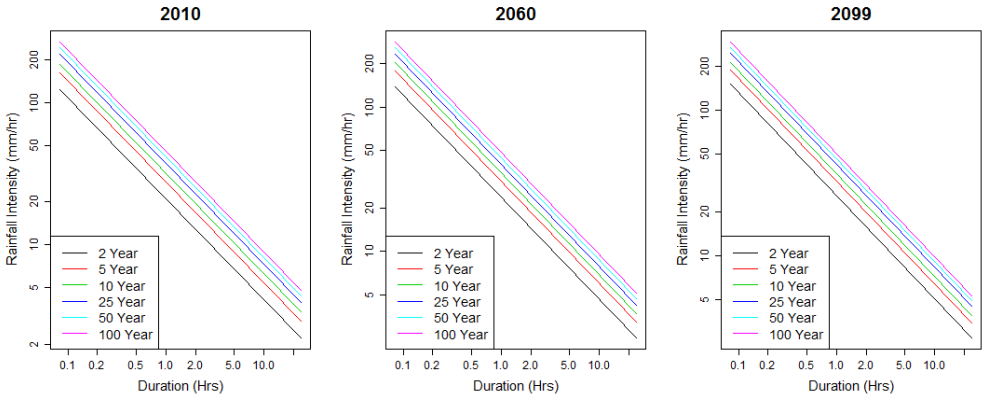

(d) MPI-ESM RCP 2.6

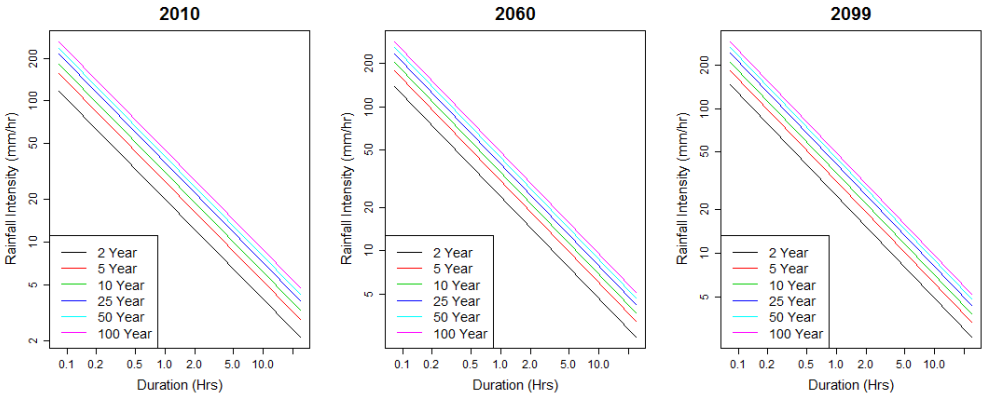

(e) MPI-ESM RCP 4.5

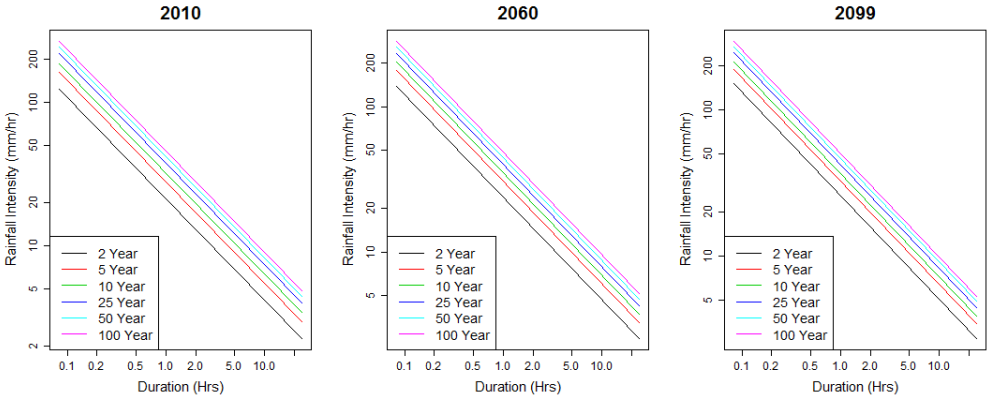

(f) MPI-ESM RCP 8.5